Journal of Petroleum Science and Engineering 205 (2021) 108914

Contents lists available at ScienceDirect

Journal of Petroleum Science and Engineering

journal homepage: www.elsevier.com/locate/petrol

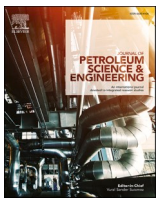

Mineralogy and geochemistry of reservoir and non-reservoir chalk from the Norwegian continental shelf

E.I. Kallesten [a,b,*], U. Zimmermann [a,b], M.V. Madland [a,b], S. Bertolino [c], E. Omdal [d], P. Ø. Andersen [a,b]

[a] University of Stavanger, Kristine Bonnevies vei 22, 4021, Stavanger, Norway
[b] The National IOR Centre of Norway, Kristine Bonnevies vei 22, 4021, Stavanger, Norway
[c] Universidad Nacional de Cordoba, Av. Medina Allende, 2144, Cordoba, Argentina
[d] ConocoPhillips, Ekofiskveien 35, 4056, Tananger, Norway

ARTICLE INFO

Keywords:
Geochemistry
Mineralogy
Reservoir chalk
North sea chalk
EOR

ABSTRACT

A first and detailed study of the geochemistry and mineralogy characterizing the North Sea reservoir and non-reservoir chalk is provided in this work. The study is based on 185 cores from exploration and development wells in the North Sea. The cores related to reservoir development have different flooding status – unflooded or waterflooded at various temperatures – and are directly sampled from the Ekofisk field. Optical petrography shows a micritic carbonate matrix, with grains represented by various microfossils such as foraminifers and sponge spicules. Scanning electron microscopy (SEM) reveals post-depositional calcite precipitation and cementation. Dolomite is found only in the reservoir samples, but it is discussed as a diagenetic feature, unrelated to the hydrocarbon content or EOR exposure. The non-carbonate minerals observed with BSE-SEM and XRD include mostly quartz but also smectite, illite, kaolinite, mica, and pyrite. The abundance of clastic input varies, and there is a clear decrease in porosity stratigraphically downwards, with stronger cementation and higher compaction. $\delta^{13}C$ reflects primary trends for Upper Cretaceous stages while $\delta^{18}O$ in all samples is lower than the secular global isotopic values for this period. However, the $\delta^{18}O$ values are not sufficiently low to imply a strong diagenetic overprint, but rather suggest the influence of a secondary fluid. This fluid cannot be a hydrocarbon-rich one, nor EOR fluids, as non-reservoir samples, as well as flooded and unflooded reservoir samples show very similar stable isotope values.

1. Introduction

Carbonate reservoirs hold significant amounts of the hydrocarbon reserves worldwide. Most of the largest Norwegian carbonate reservoirs are found in the North Sea, an intracratonic basin on the Norwegian Continental Shelf (NCS) formed as the result of several major tectonic events between the Devonian and Late Jurassic. The reservoirs are chalk deposits developed predominantly by sedimentation of planktonic carbonate algae – coccolitophorids – during the Upper Cretaceous into the Paleocene (Faleide et al., 2010).

Since the discovery of the Ekofisk field in 1969, the chalk play remains among the most prolific hydrocarbon resources in the North Sea, Ekofisk field alone accounting for approximately 10% of the produced net oil equivalents on the NCS. After the primary oil recovery, the initiation water injection program on Ekofisk in 1987 the seawater has been remarkably efficient for oil recovery, leaving water flooded zones with irreducible oil saturation of around 30%. However, even with this good recovery already achieved, the amount of the resources left behind in the flooded zones is significant, simply due to the size of the reservoirs. This rose the motivation for studying the factors that govern this oil replacement.

For economic and availability reasons, much of the extensive research for enhanced oil recovery (EOR) on the NCS involves outcrop samples. Yet, studies showed that, despite the predictable mineralogical and petrological aspects of this rock type, factors such as depositional environment, specific diagenetic history, can strongly influence engineering properties of chalk (Scholle, 1977; Brasher and Vagle, 1996; Hjuler and Fabricius, 2009; Minde et al., 2016), and hence a direct transfer of data from one chalk type to another is not always applicable. Although the Ekofisk discovery initiated several studies on North Sea

* Corresponding author. University of Stavanger, Kristine Bonnevies vei 22, 4021, Stavanger, Norway.
E-mail address: emanuela.i.kallesten@uis.no (E.I. Kallesten).

https://doi.org/10.1016/j.petrol.2021.108914
Received 17 March 2020; Received in revised form 29 March 2021; Accepted 2 May 2021
Available online 10 May 2021

chalk (Van Den Bark and Thomas, 1981; D'Heur, 1991; Herrington et al., 1991) field observations and further laboratory studies also show that production-related processes, such as changes in reservoir stress state, or waterflooding for EOR purposes, can further influence chalk properties (Bjørlykke and Høeg, 1997; Sylte et al., 1999; Madland et al., 2011) and that the extent of the rock-fluid interactions are closely related to the rock mineralogy (Andersen et al., 2018; Madland et al., 2011; Minde et al., 2018; Strand et al., 2007; Kallesten et al., 2020).

There are very few previously published contributions that characterize the North Sea chalk and support forecasts of the impact the EOR methods have on North Sea chalk (e.g., Scholle, 1974; Egeberg and Saigal, 1991; Stoddart et al., 1995; Hjuler and Fabricius, 2009; Gennaro et al., 2013) and very often porosity, permeability models of North Sea chalk are mostly based on rather limited data sets (Jensen et al., 2000; Talukdar et al., 2002).

Therefore, the main objective of this study is a thorough characterization of North Sea chalk in terms of geochemistry and petrology and thus provide insight on key-aspects of North Sea chalk properties relevant for hydrocarbons production, such as chemical composition, mineral structures and textures and diagenetic overprint of the North Sea chalk. A novel aspect of the study is that the sample set includes an extraordinary assembly of 185 chalk cores from various locations in the North Sea from exploration and development wells, both with and without hydrocarbon content (referred to hereafter as reservoir and non-reservoir, respectively). The reservoir cores have various flooding statuses, both exposed to seawater injection (flooded) and not exposed to EOR fluids (unflooded). Therefore, besides the general characterization, we aim to evaluate the impact of hydrocarbons on the petrological, mineralogical and geochemical properties of the chalk as well as the impact of water-related EOR methods on chalk by comparing analytic results from waterflooded cores at various temperatures to unflooded reservoir cores, a study that has never been carried out.

The outcome of this study can serve as a standard in validating the relevance of outcrop chalk research for the North Sea context, and for selecting a suitable outcrop chalk analogue for further research; it can also contribute to increased model accuracy and refined experimental designs for EOR purposes.

2. Sample set

We present extensive analytical studies on chalk successions from 11 different wells in the North Sea, including reservoir chalk from the Ekofisk area and non-reservoir chalk cores from exploration wells in the Ekofisk area and other areas further North, such as Varg, Ragnarock and Balder/Grane. The wells are numbered 1 to 11, from south to north (Fig. 1, left). The samples from wells 1–5 are horizontal core plugs (drilled parallel to bedding) of reservoir chalk from the Tor Formation and Ekofisk Formation (Upper Cretaceous, Paleocene, Fig. 1, right) and have different flooding statuses linked to hydrocarbon production – unflooded and water-flooded. The flooding fluid is seawater and the fluid temperature is not defined beyond hot and cold; also, the exact distance between the flooded cores and the injectors is not given, but it can be assumed that they have been flooded over several years at high flooding rates. Due to the confidential nature of wells 1–5, their actual ID number and exact geographic position remain undisclosed.

The chalk successions from wells 6–11 were provided by Norwegian Petroleum Directorate (NPD) in Norway and cover mainly the Tor Formation with few from the underlying Hod Formation (Campanian, Upper Cretaceous) and the overlying Ekofisk Formation. Wells 6–11 are exploration wells and most of the cores from these wells are hydrocarbon-free (non-reservoir). Their location and ID are shown in Fig. 1 and Table 1. However, wells 6 and 7 contains partly confidential cores and therefore their well ID remains undisclosed. Table 1 shows an overview of the number of reservoir and non-reservoir core plugs related to each well, the formations they represent, and details related to the flooding status of the reservoir cores.

3. Methods

The study is based on several analytical methods, and an overview of the measurements is listed in Table 2.

3.1. Separation of the non-carbonate fraction

23 samples from wells 1–4 were selected to separate the carbonate fraction from the non-carbonate material. For this, the samples have been treated with weak acetic acid (2 M concentration) for several days. They were then filtered, dried and again treated with acetic acid until the carbonate content was relatively low. The insoluble residue (IR) was used for geochemical analyses and XRD measurements.

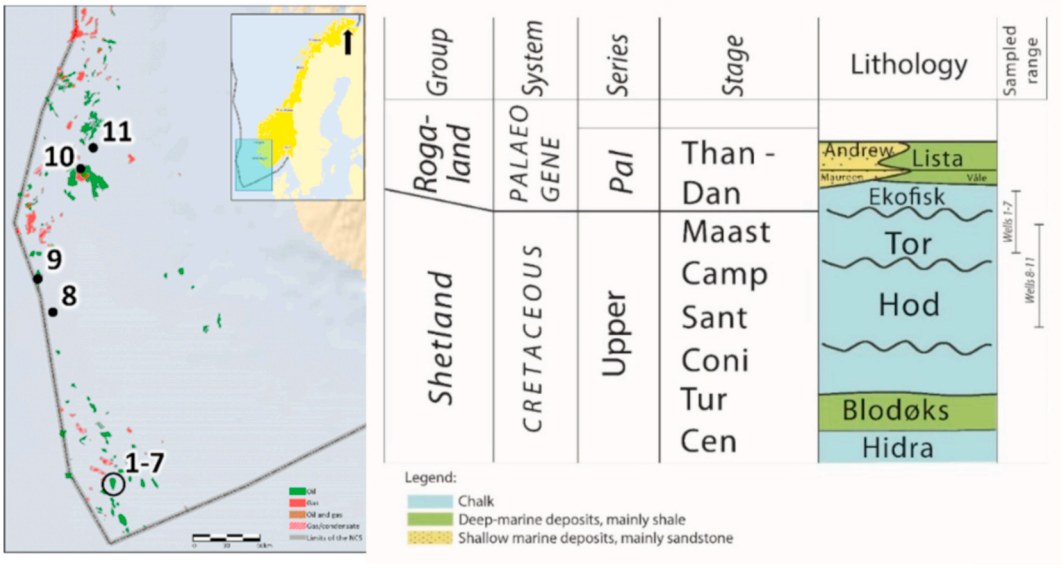

Fig. 1. Left: Close-up of the shaded area in the inset map representing the section of Norwegian Continental Shelf and the approximate location of the wells in this study; Right: excerpt from lithostratigraphic chart of the North Sea. (source: npd.no).

Table 1
Overview of the sample set; well ID undisclosed for wells 1–7. Wells 6, 7 and 10 contain both reservoir and non-reservoir samples. * - including cores with unknown flooding status.

Well number	Well ID	Type	Formation	Reservoir cores	Non-reservoir cores	Flooded cores	Unflooded cores
1	–	Development	Tor	51	–	33	18
2	–	Development	Tor, Ekofisk	13*	–	9	–
3	–	Development	Ekofisk	12	–	6	6
4	–	Development	Ekofisk	23	–	7	16
5	–	Development	Tor, Ekofisk	3	–	–	3
6	–	Exploration	Tor, Ekofisk	6	2	–	–
7	–	Exploration	Tor, Ekofisk	30	19	–	–
8	7/1-1	Exploration	Hod, Tor	–	8	–	–
9	15/12-4	Exploration	Tor	–	5	–	–
10	16/2-3	Exploration	Hod, Tor	2	9	–	–
11	25/11-17	Exploration	Tor	–	4	–	–

Table 2
Overview of applied methods and number of measurements; Thin sections – TS, Scanning electron microscopy – SEM, X-ray diffraction – XRD, Insoluble residue x-ray diffraction – IR-XRD, Geochemistry – GC, Insoluble residue geochemistry – IR-GC, Carbon and oxygen stable isotope – C–O; *-measurements involving cryo-SEM.

	Well						
	Methods and number of measurements						
	TS	SEM	XRD	IR-XRD	GC	IR-GC	C–O
1	15	8	16	6	19		48
2	3	3	9	4	13		13
3	12	7*	12	5	12	5	39
4	7	4	11	8	13		22
5	3		10		12		3
6	3	1			8		10
7	11	1			47		128
8	2	1			10		8
9	2	1			4		5
10	1				5		7
11					3		3

3.2. Optical petrography

The characterization methods include optical petrography of polished thin sections of 40 reservoir and 19 non-reservoir cores for first data about the texture and the composition of the chalk (Zeiss AXIO polarized microscope, University of Stavanger).

3.3. Field emission gun scanning electron microscope (FEG-SEM) with cryogenic unit (cryo-SEM) backscattered electron detector (BSED) and energy dispersive system (EDS)

Fresh surface fragments from five uncleaned reservoir cores (2 unflooded and 3 water-flooded from well 3) were analysed under cryogenic conditions to avoid contaminating the SEM column. The procedure included lowering the samples into nitrogen slush (i.e., liquid nitrogen cooled under vacuum conditions) for rapid freezing, measure taken in order to avoid the vaporization of the hydrocarbons during electron scanning, and consequently contamination of the SEM column. The analysis took place at the University of Stavanger, using a Zeiss Supra 35VP SEM, equipped with a Polar Prep 2000T cryo- SEM system.

An additional SEM and BSED study of polished thin sections took place at Technical University in Freiberg (18 reservoir thin sections from wells 1–4) and University of Stavanger (two non-reservoir thin sections from wells 8 and 9).

3.4. Stable isotope

The analytical work also includes stable carbon and oxygen isotope geochemistry (VG Isoglas PRISM III stable isotope ratio mass spectrometer, Wolfson Laboratory, Edinburgh University). The subsamples are fine powder, mainly from fresh surfaces. The carbonate powder was reacted with 100% orthophosphoric acid at 90 °C in an ISOCARB automatic carbonate preparation system. To test possible artefacts related to drilling, probes obtained from core sides were included, in addition to fresh surface. The data set includes 125 C and O isotope ratios from the reservoir chalk and 162 from the non-reservoir cores. Both oxygen- and carbon-isotopic data are reported in units per mil notation (‰) relative to the Vienna Pee Dee Belemnite (V-PDB) standard. The standard deviation of the powdered coral laboratory standard (COR1D, $\delta^{13}C_{PDB} = -0.648$, $\delta^{18}O_{PDB} = -4.920$) run as a sample on the same days as the study samples was $\pm$ 0.04‰ for $\delta^{13}C$ and $\pm$ 0.06‰ for $\delta^{18}O$.

3.5. X-ray diffraction

X-ray diffraction (XRD) was used for mineral identification and relative quantification of reservoir samples. The bulk samples were carefully hand-milled in an agate mortar to very fine powder. 12 bulk samples and 5 insoluble residue from well 3 were measured at Instituto Jaime Almera - C.S.I.C.Barcelona (Spain), where the XRD patterns were obtained from a Bruker D5005 diffractometer, Cu Kα x-ray radiation at 40 mA and 40 kV intensity, 0.1 mm receiving slit size. The measurement was between 3 and 65° 2Θ in increments of 0.02° 2Θ, 6 s per increment. The remainder of the samples (55 bulk rock and 17 insoluble residue) were measured at University of Stavanger, in a Bruker D8 ADVANCE ECO diffractometer with a Lynxeye detector, Cu Kα x-ray radiation at 40 kV and 25 mA intensity, 0.6 mm receiving slit, 4–70° 2Θ in increments of 0.01°, 0.2 s per increment. Mineral identification was performed on DIFFRAC.EVA software for semi-quantitative relative mineral proportions of whole rock patterns while for the siliciclastic fraction quantitative mineral proportions were obtained by Rietveld refinement with TOPAS5®.

Material from non-reservoir samples was not available for XRD measurement.

3.6. Geochemistry

Major, trace and rare earth elements geochemistry analysis took place at Acme Laboratories (Canada). The method analysed machine-milled fine powder from 69 reservoir and 77 non-reservoir cores. The material was milled and analysed at Bureau Veritas Minerals laboratories in Canada. The samples were ground in an agate mill and then mixed with $LiBO_2/Li_2B_4O_7$ flux in crucibles and fused in a furnace. The resulted bead was cooled and dissolved in ACS grade nitric acid and analysed by Inductive Coupled Plasma-Mass Spectrometry (ICP-MS). Loss on ignition (LOI) was determined by igniting the sample with a known mass in a tarred crucible at 1000 °C for 1 h and calculating the difference in mass after the sample was cooled. Total Carbon and Sulfur were determined by the LECO® method. An additional 14 elements

were measured after dilution in Aqua Regia solution of equal parts concentrated HCl, HNO_3, and DI-H_2O for 1 h in a heating block or hot water bath. The sample volume was increased with dilute HCl-solutions. All measured concentrations were in the standard range of the possible detection limit, accuracy was between 1 and 2%. Further measurement and processing details can be found at http://acmelab.com.

4. Results

4.1. Optical petrography

As chalk is very fine-grained, optical microscopic analyses are restricted to only some specific features. All thin sections reveal a mud supported fabric. All three formations (Hod, Tor and Ekofisk) contain a similar faunal group assemblage, including mainly a large variety of calcareous nano-, micro- and macrofossils (foraminifera, bivalves, crinoid stem fragments) and siliceous sponges (Fig. 2a). There is no visible distinction between reservoir (Fig. 2, left column) and non-reservoir samples (Fig. 2, right column) nor between flooded and unflooded samples in terms of texture and fabric. The samples can be classified as mud- to wackestone according to Dunham carbonate classification (Dunham, 1962) but local accumulations of fossils are common (Fig. 2b).

Foraminifer tests appear intact, either calcite filled or hollow. Samples from Ekofisk Formation show a notable variation, as the fauna changes from mostly calcareous fossils to predominantly sponge spicules in wells 3 and 7 (Fig. 2c and d respectively). The sponge spicules are mostly elongated rays (monaxone, Fig. 2d), but triaxone spicules are also present (Fig. 2c), with moldic voids filled with calcite after the original silica leached. They are often oriented, oblique to the drilling direction.

Stylolites occur in samples from both Tor and Ekofisk Formations, with the distinct serrated surface made visible by a change in color, related to the clay minerals fill (Fig. 2e). Fractures and fissures appear in samples from all wells, they are mostly calcite-cemented, but are also sometimes filled with an opaque, dark material that optical petrography cannot identify (Fig. 2f).

4.2. Electron microscopy and energy dispersive spectroscopy

Cryo-SEM micrographs of fresh core surfaces from well 3 (Fig. 3) show textural and compositional similarities between the water-flooded and unflooded cores. The main constituent of the deposit is the matrix composed of 1–2 μm size calcite crystals from broken, disaggregated coccoliths, but also intact coccolith platelets and coccolithosphores. The samples have intraparticle porosity, but although the many foraminifera may have retained their globular shape, some are deformed, broken, and the pore spaces are filled with new calcite crystals (Fig. 3a and b), or

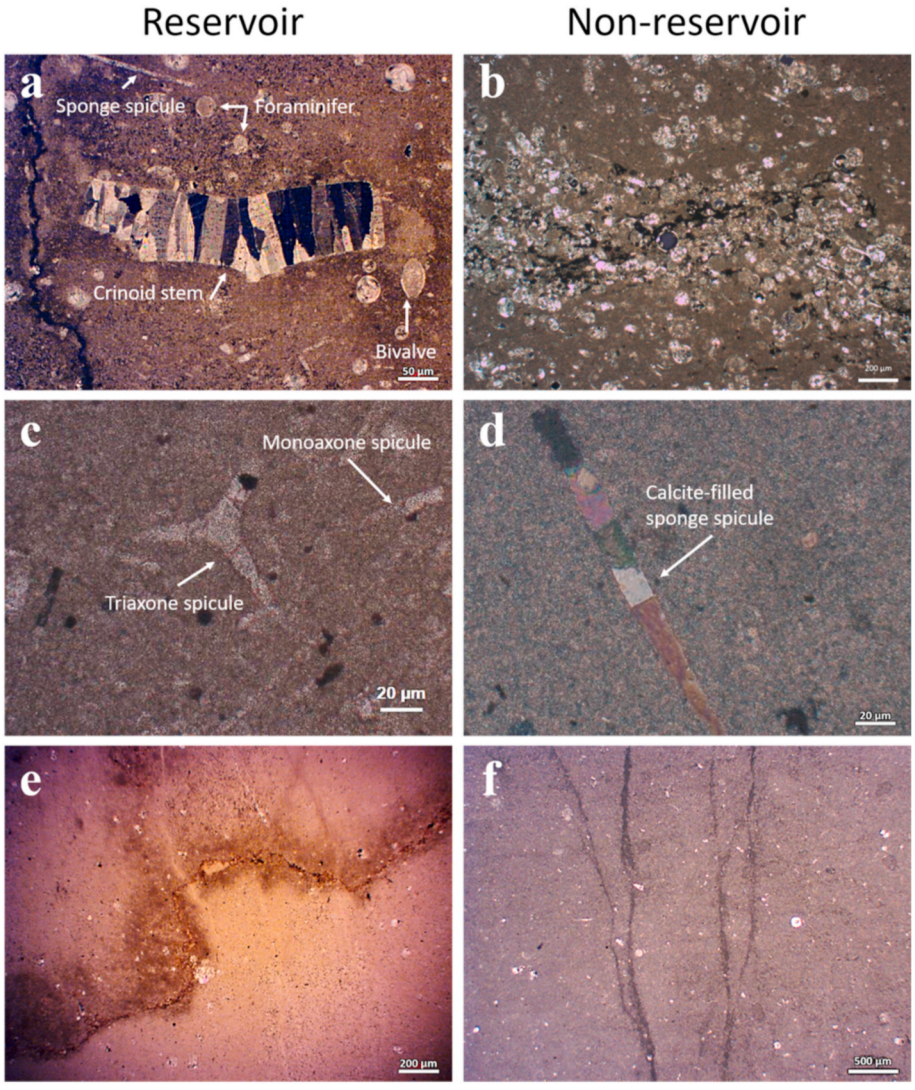

Fig. 2. Micrographs showing various features in thin sections from Ekofisk Formation (a–d) and Tor Formation (e, f) representing both reservoir (left column) and non-reservoir (right column) samples; (a) plane polar micrograph of crinoid stem fragment (center), calcite-filled foraminifers of various sizes and sponge spicules; stylolite section to the left (well 1); (b) accumulation of foraminifers along stylolite (Ekofisk Formation, well 7); (c) calcite-filled triaxone spicule (center) and monoaxones (well 3); (d) cross polar view of calcite- filled sponge spicule (Ekofisk Formation, well 7); (e) stylolite (well 1, Tor Formation); (f) braided veins filled with opaque material (plane polar view, well 6).

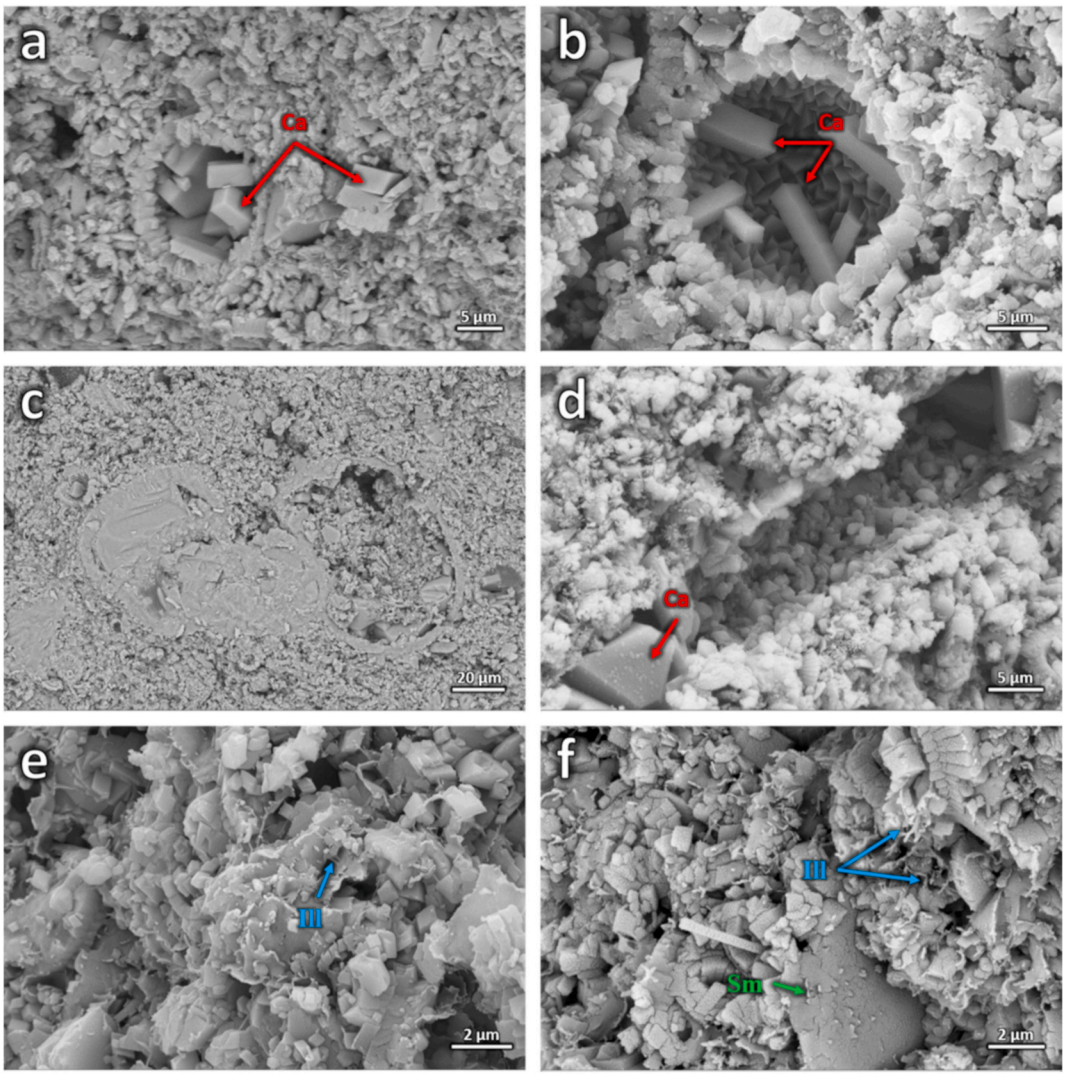

Fig. 3. Cryo-SEM micrographs of waterflooded and unflooded reservoir core plug from well 3: a - new calcite crystals precipitated inside foraminifer cavity and inside an homogenous matrix (Ca, red arrows; waterflooded sample); b - new calcite crystals precipitated inside cavity of well-preserved foraminifer test (Ca, red arrow; unflooded sample); c – foraminifer chambers entirely filled with calcite or cocolith debris (waterflooded sample); d - cavity left after leaching of sponge spicule, with new calcite crystal growth (Ca, red arrow, waterflooded sample)); e – inhomogeneous unflooded sample with bridge of acicular illite joining flakes (Ill, blue arrow); f - inhomogeneous unflooded sample (same as featured in 4e) with authigenic acicular illite (Ill, blue arrows) and smectitic clays (Sm, green arrow). (For interpretation of the references to color in this figure legend, the reader is referred to the Web version of this article.)

coccolith debris (Fig. 3c). The void left after the sponge silica dissolved is entirely or sometimes partially filled with calcite crystals (Fig. 3d).

Both waterflooded and unflooded samples contain non-carbonate minerals such as quartz, biotite, muscovite, pyrite, kaolinite, or apatite. The minute amount and variety are similar in all samples but one (unflooded), which stands out with more abundant clay minerals than the others, and consequently a less homogeneous texture (Fig. 3e and f). SEM micrographs of this sample show a conspicuous occurrence of clay flakes bent with irregular and curly edges, all features of detrital smectitic clays such as mixed layers illite-smectite and chlorite-smectite (Fig. 3f, green arrows) also suggested by the x-ray diffraction (XRD) band around 5°–9° 2Θ and the wide band at the position of illite and chlorite (8.7° and 12.3° 2Θ respectively). The flakes are also coating surfaces of voids. There is also authigenic, acicular shaped illite eventually in bundles (Fig. 3f, blue arrows) that seem to be growing from smectitic clays. The blue arrow in Fig. 4e marks a bridge of acicular illite joining flakes.

In comparison, Fig. 3b, also of an unflooded sample, exhibits completely different clay features compared to Fig. 3e and f. Clays are minuscule and less frequent, thus hard to distinguish in the SEM images.

4.3. Backscatter electron analysis of thin sections

4.3.1. Reservoir samples

Further SEM and BSED analyses of thin sections reveal a similar mineral content in reservoir wells 1, 2 and 4 as seen in cryo-SEM analyses of well 3 cores. Besides calcite as the main constituent, dolomite ($CaMg(CO_2)_3$) is present in all reservoir wells, and in both formations, regardless of the flooding status (flooded at either hot or cold temperature, or unflooded). It appears both as new crystals, precipitated *in-situ*, with an ankerite ($CaFe(CO_2)_3$) rim (Fig. 4a) along fractures, stylolite seams, or in pores, and as cement filling of fossils.

Veins and fractures observed in the studied samples are often calcite-cemented, but a reworked material consisting of brecciated calcite fragments, quartz, kaolinite and dolomite crystals sometimes line the fracture walls (Fig. 4b), partially reducing the fracture apertures. This represents the dark, opaque material that could not be identified by optical microscopy. Further, kaolinite and quartz often occur in the existing inter- and intraparticle pore spaces.

Framboidal pyrite (Fig. 4c) is also common in all reservoir cores, often in residual stylolite seams, veins and fractures (Fig. 4d) or as

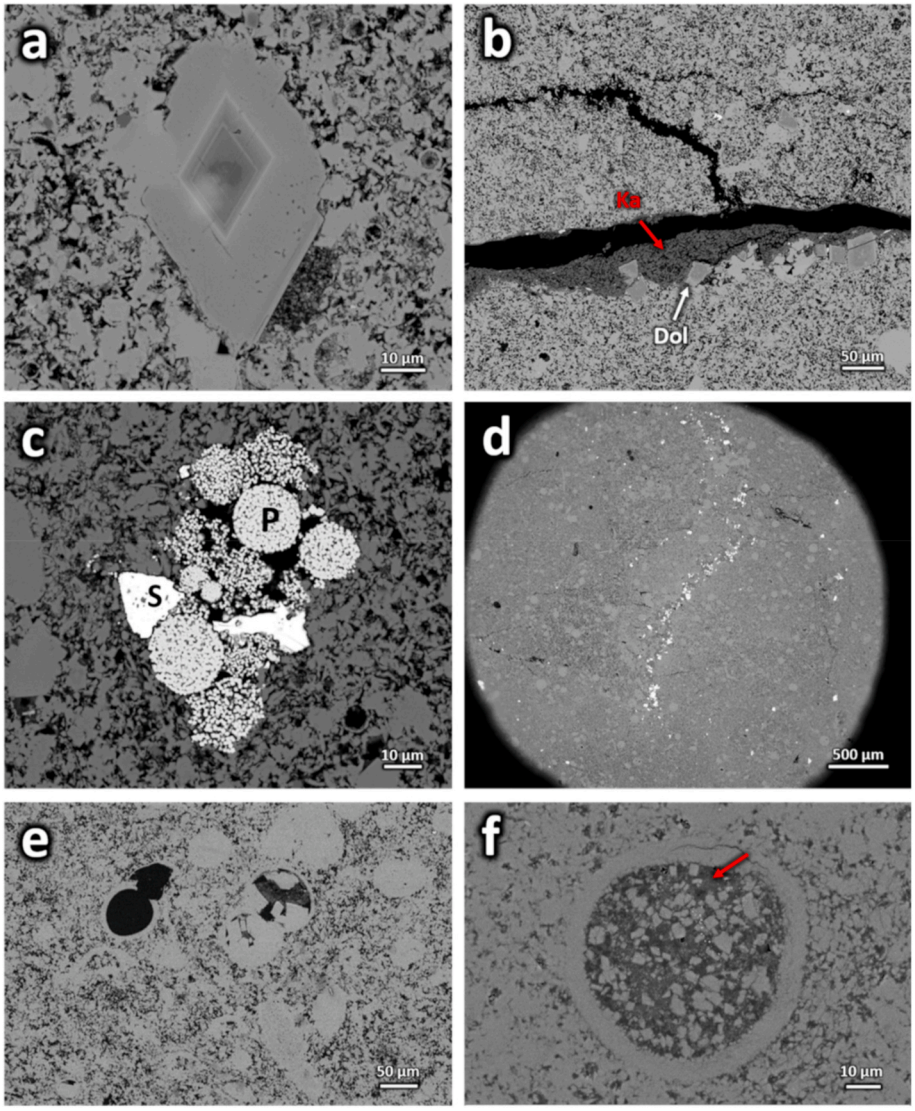

Fig. 4. BSE micrographs of a – secondary dolomite crystal with light ankerite rim (unflooded sample, well 3); b – kaolinite (Ka, red arrow) and in-situ dolomite crystals (Dol, white arrow) along fracture walls(unflooded sample, well4); c – framboidal pyrite (P) and (S) sphalerite (unflooded sample, well 4); d – bright pyrite along stylolites (cold waterflooded sample, well 1); e – foraminifers from empty to fully cemented with calcite in coccolith matrix (well 8); f – foraminifer filled with aluminosilicate phase (red arrow, well 9). (For interpretation of the references to color in this figure legend, the reader is referred to the Web version of this article.)

scattered crystals.

Apatite is here mostly linked to vertebrate remains (fish bones, scales, teeth) but occurs also as primary, detrital phase. Muscovite, biotite and albite are present as minute authigenic crystals in interparticle pore spaces. Sphalerite incapsulated in pyrite (Fig. 4c), fluorite precipitates in cavities, and cassiterite, minerals associated with hydrothermal activity (Howie et al., 1992) appear in several of the thin sections.

4.3.2. Non-reservoir samples

The non-reservoir samples reveal similarities to their reservoir counterparts in terms of the faunal content, texture, mineral assemblage, and relative mineral proportions. Pelagic foraminifers are present, their chambers can be empty, but often are filled (partially or entirely) with precipitated calcite crystals (Fig. 4e).

Analysed thin sections of non-reservoir cores did not contain dolomite. Re-worked material consisting of quartz and kaolinite, similar to what was observed in reservoir samples is present in veins and pore spaces in samples from wells 7, 8 and 9. This material contains magnesium, but it is not associated with dolomite, but rather associated to an aluminosilicate phase (Fig. 4f).

4.4. X-ray diffraction (XRD) of bulk and insoluble residue samples

The measurement covers bulk and insoluble residue samples from wells 1–5.

Besides the high calcite content, whole-rock XRD scans confirm quartz as an accessory mineral in all reservoir samples. None of the silica content is related to opal. The restricted mineral assemblage is similar in all reservoir samples, both unflooded and waterflooded, but their relative abundance varies as follows:

4.4.1. Well 1

Samples at the top of the succession (cold-waterflooded) contain 90–95% calcite, with quartz varying between 5 and 8%. The samples contain traces of dolomite (or ankerite), phylosilicates and halite. Samples that were flooded at high temperature contain the same calcite proportion as the cold-waterflooded samples; the non-carbonate fraction consists of quartz (7–8% of the bulk rock) and traces of 7 Å (d) mineral such as kaolinite or chlorite. The unflooded samples contain a higher amount of calcite (close to 100%) than the flooded samples. Quartz is the only non-carbonate mineral detected and the highest amount (3%) is found in one of 6 unflooded samples, other samples only showing scarce or traces of quartz.

4.4.2. Well 2

Besides 2 samples, all measured samples from well 2 contain approximately 100% calcite and traces of dolomite. These two exceptions contain 88% and 90% calcite, and respectively 12% and 10% non-carbonate minerals. The 10% siliciclastic fraction consists of 92% quartz and 8% of clay minerals such as chlorite and smectitic clays (mixed layer clays mostly) and traces of hematite. The siliciclastic fraction of the lowest stratigraphic sample in this well has less amount of quartz (65%) and 18.6% of clay minerals (chlorite and smectitic, mixed layer) and minor barite as well as analcime.

4.4.3. Well 3

All samples contain dominant calcite (85–90%) along with quartz (10–15%) and traces of dolomite or ankerite, halite and phyllosilicates. In the siliciclastic fraction quartz is the dominant phase (67.4%–85.2%) along with clays and micas (11.2%–32.1%) and other minerals such as plagioclase (in both waterflooded and unflooded samples) and amphibole. Clays are mostly smectite and smectitic mixed layer clays (illite-smectite I/S and chlorite-smectite C/S), illite, chlorite and kaolinite (the two latter identified in 4 out of 5 measured samples).

4.4.4. Well 4

The eight unflooded samples from well 4 contain 94–98% calcite with minor quartz. Three of these also contain scarce to traces of dolomite (and/or ankerite), and scarce halite and minor barite. The siliciclastic fraction of the highest laying unflooded sample is composed of mainly phyllosilicate minerals, mostly clay minerals dominated by smectitic minerals (most likely mixed layer -ML- clays I/S and chlorite/smectite), kaolinite, traces of chlorite associated with abundant quartz and scarce amounts of other minerals such as plagioclase, gibbsite, gypsum and halite.

The waterflooded samples contain dominant calcite (approximately 95–98%) and scarce quartz and dolomite (and/or ankerite); halite is also noticeable. The siliciclastic fraction of the highest laying waterflooded sample is dominated by quartz with minor clay minerals (mostly smectitic, mixed layers, and minute kaolinite), rare plagioclase and other minerals like fluorapatite and hollandite or proto-enstatite could be identified. One of the waterflooded samples on the other hand has a different assemblage: dominant clay minerals (clinochlore and smectitic and mixed layer clays along with minor kaolinite), associated with quartz minor plagioclase.

4.4.5. Well 5

The four measured samples from the top of the succession in this well contain approximately 77–79% of calcite, 17–18% of quartz and scarce dolomite (and/or ankerite), kaolinite and halite. The rest of the samples are all quite similar: almost entirely consisting of calcite with $\leq$2% of quartz and traces of dolomite.

4.5. Whole-rock geochemistry

Major, minor and trace element concentrations listed in Tables 3–5 are valuable indicators for key aspects such as depositional environments and diagenetic overprint.

Major element geochemistry of the whole rock analysis from all wells shows a large variation in the silica (SiO_2) content with values ranging from 0.3% up to 20%. Samples with higher silica content than 10% are arbitrarily classified as marl and marked in bold in Tables 3 and 4, while those with silica content between 5 and 10% are classified as marly chalk and marked in italics. Table 3 shows selected element concentrations from wells 1–5 containing exclusively reservoir samples and includes information of their flooding status. The elemental concentrations for reservoir and non-reservoir samples from wells 6–11 are shown in Table 4. Element concentrations of insoluble residue from samples in well 3 are listed in Table 5.

Wells 1, 2, 4 and 6 carry mainly clean chalk and only very few marls at the top of the sampled range. However, well 3 has consistently higher silica abundances between 5 and 10%, representing between 67 and 75% of the non-carbonate phase (Table 5). Wells 2, and 5 contain a large amount of clastic material in the Ekofisk Formation but in the underlying Tor Formation clean chalk occurs. Well 7 shows this change at a deeper level, at the top of the Tor Formation.

MgO is slightly enriched with values above 0.4% in only some chalk samples and in such cases, this correlates with an enriched silica content pointing to clay minerals or other clastic phases. However, in wells 4 and 5 MgO is clearly more abundant in all lithotypes even in clean chalks but does not correlate with silica.

No other major element shows any significant abundance in chalk samples. In marls and marly chalk (in bold, respectively italics in Table 3) Al_2O_3 and Fe_2O_{3t} are enriched together with silica pointing to feldspar and phyllosilicate abundance.

Clastic input can be monitored by certain trace elements, like rubidium (Rb) and zirconium (Zr), which occur solely in clastic material and are absent in carbonates. Their abundance together with Rare Earth Elements (REE), which are extremely depleted in all chemical sediments, would, when enriched, point to phyllosilicates or apatite, both enriched in the latter. Rb and Zr values in chalk samples are mostly below 2% of the typical values for the Post Archaean Australian Shale (PAAS; after Taylor and McLennan, 1981) with threshold values of 4.2 ppm for Zr and 3.2 ppm for Rb (Frimmel, 2009). This applies to nearly all samples in the wells 1–7. Only in well 7 from the Ekofisk area some chalk samples are enriched in Zr, while this trend is very pronounced in all sampled wells 7–11 further North (Table 4).

The REE and yttrium (Y) concentrations normalized to the PAAS values reflect a general depletion of the REE by an average factor of 6 (Figs. 5 and 6). The enrichment in lanthanum (La), depletion of cerium (Ce) and a positive Y anomaly are a typical signature for influence of open marine seawater during precipitation of the carbonate (Bau and Dulski, 1996; Nozaki et al., 1997; Bau and Alexander, 2006). Shale-normalized REE plots of reservoir chalk samples (Fig. 5; blue lines) and non-reservoir chalk samples (Fig. 6; blue lines) have partly a typical pattern for seawater with a positive anomaly of La (calculated as 3xPr – 2xNd) and a pronounced positive Y anomaly. At the same time, middle REE (Sm – Ho) should not be enriched in carbonates (Nozaki et al., 1997), and the only few chalk samples that show this feature also contain elevated Zr concentrations (6–7 ppm). Marly chalk samples (Figs. 5 and 6; yellow lines) generally show a transition between typical REE pattern for chalk and a more enriched middle REE pattern for marls (Figs. 5 and 6; grey lines).

Total REE (ΣREE) in chalk samples are mostly below 30 ppm and there are trends within the wells. Well 1 shows a variation between 10 and 33 ppm, so do samples from well 4 (17–36 ppm), while samples in wells 2, 6, 7 (18–30 ppm) and 5 (41–43 ppm) have a narrower range. Well 3 is affected by clastic material and among the marly chalks ΣREE varies immediately between 39 and 47 ppm. ΣREE from the northern wells 8, 9 and 10 are very variable (15–68 ppm) while samples from well 11 registered ΣREE well below 20 ppm. High Zr concentrations correlate partly with enriched ΣREE, but not in all samples.

Marly chalk and marl samples have mostly elevated ΣREE generally between 40 and 60 ppm, with one exception of a samples from well 7 which contains less than 30 ppm. Marls are significantly higher with values up to 200 ppm. The non-carbonate phase separates are comparable to shales with value close to, but often a slightly below a typical PAAS composition of 183 ppm (Taylor and McLennan, 1981).

Samples affected by clastic input are neglected when analyzing specific REE values for yttrium/holmium (Y/Ho) ratios. Y/Ho (Fig. 7) average between 38 (Ekofisk Formation; blue markers) and 40 (Tor Formation; green markers) in the reservoir samples and appear slightly lower in the non-reservoir samples, averaging at 34 (Hod Formation, black markers) and 38 (Tor Formation, yellow markers). The same ratio calculated on the non-carbonate fraction composition (Table 5) has an average of 32, which is close to PAAS values. The reservoir chalk Y/Ho

Table 3
Major, minor and trace element concentrations in samples from reservoir wells 1–5; Fm – formation; dl - detection limit; bdl - below detection limit; WF - waterflooded (c-cold, h-hot); UF – unflooded; italics – marly chalk; bold – marl.

Well	Flooding status	Fm	SiO2	Al2O3	Fe2O3	MgO	CaO	Rb	Sr	Zr	Y	Ho	ΣREE
			%	%	%	%	%	PPM	PPM	PPM	PPM	PPM	PPM
		dl	0.01	0.01	0.01	0.01	0.01	0.1	0.5	0.1	0.1	0.02	
Well 1	WF-C	EKO	1.83	0.11	0.17	0.83	51.41	1.6	1242.7	1.7	6.5	0.15	17.04
		EKO	4.78	0.29	0.29	1.23	48.91	2.1	1124.1	3.3	9.4	0.23	28.19
		EKO	2.75	0.12	0.21	0.75	51.30	1.5	1213.1	1.9	7.1	0.16	18.74
		EKO	2.39	0.08	0.11	0.52	52.01	1.2	1328.9	1.6	5.6	0.14	15.58
		EKO	2.19	0.13	0.38	0.48	52.60	1.2	1388.7	1.8	10.2	0.27	29.28
	WF-H	*TOR*	*8.67*	*0.69*	*0.22*	*0.25*	*47.22*	*3.1*	*1097.0*	*4.9*	*13.3*	*0.35*	*45.12*
		TOR	*6.97*	*0.45*	*0.31*	*0.26*	*48.52*	*1.5*	*1188.2*	*4.6*	*14.8*	*0.38*	*46.74*
	WF	*TOR*	*5.06*	*0.46*	*0.15*	*0.22*	*49.77*	*1.8*	*1249.3*	*3.2*	*13.5*	*0.35*	*40.87*
		TOR	3.14	0.25	0.17	0.23	51.34	0.6	1246.8	2.9	10.6	0.30	30.39
		TOR	3.66	0.30	0.16	0.22	50.70	1.5	1335.7	2.3	12.0	0.30	33.46
	UF	TOR	0.41	0.02	0.06	0.20	51.37	0.7	1677.2	0.8	6.9	0.13	13.66
		TOR	0.39	0.03	0.06	0.20	50.93	0.6	1562.9	0.9	5.6	0.10	9.93
		TOR	0.45	0.03	0.07	0.21	49.89	0.6	1604.3	1.2	5.6	0.11	11.70
		TOR	2.53	0.20	0.12	0.24	48.22	1.4	1357.4	3.2	9.2	0.22	26.24
		TOR	2.16	0.30	0.15	0.25	48.54	1.0	1275.7	3.5	10.1	0.24	29.79
		TOR	1.01	0.11	0.07	0.22	50.39	0.1	1496.2	1.8	7.0	0.16	15.01
		TOR	0.69	0.08	0.07	0.22	50.29	0.1	1443.6	1.4	6.6	0.14	18.95
		TOR	0.68	0.06	0.09	0.21	50.08	0.7	1483.6	1.4	6.0	0.12	13.54
		TOR	0.43	0.03	0.07	0.19	50.89	0.6	1490.1	0.9	5.4	0.13	10.09
Well 2	WF-C	**EKO**	**15.34**	**1.21**	**0.33**	**0.23**	**42.49**	**5.0**	**1138.0**	**9.1**	9.9	**0.30**	**46.32**
		EKO	*9.59*	*1.44*	*0.48*	*0.38*	*45.17*	*4.9*	*1062.5*	*9.0*	14.4	*0.42*	*62.81*
		EKO	4.28	0.31	0.14	0.38	49.20	2.4	921.3	8.2	7.9	0.19	20.78
		EKO	**11.36**	**0.39**	**0.23**	**0.40**	**46.56**	**1.5**	**1120.0**	**4.9**	12.1	**0.35**	**41.90**
		EKO	**19.22**	**0.53**	**0.27**	**0.28**	**43.00**	**1.5**	**998.3**	**5.3**	12.5	**0.35**	**53.75**
		EKO	1.83	0.22	0.07	0.27	51.10	0.6	1094.8	4.4	10.7	0.27	27.68
		EKO	**19.22**	**0.53**	**0.27**	**0.28**	**43.00**	**1.5**	**998.3**	**5.3**	12.5	**0.35**	**53.75**
		EKO	1.00	0.11	0.05	0.27	53.61	0.2	1444.3	3.6	11.8	0.28	26.02
		EKO	1.34	0.17	0.09	0.26	51.11	1.1	1329.9	2.2	11.5	0.28	29.74
		TOR	2.03	0.17	0.06	0.40	50.86	0.7	1268.3	4.0	10.2	0.21	23.62
		TOR	1.61	0.17	0.07	0.34	50.87	0.2	1219.1	1.7	8.9	0.21	25.29
		TOR	1.65	0.14	0.08	0.44	50.77	0.2	1484.9	2.6	9.6	0.22	23.98
		TOR	1.14	0.13	0.07	0.45	52.95	0.2	1505.0	1.7	9.5	0.21	21.82
Well 3	UF	**EKO**	**10.81**	**1.69**	**0.34**	**0.41**	**46.17**	**6.5**	**1197.0**	**6.5**	**13.6**	**0.42**	**55.28**
		EKO	*6.81*	*0.44*	*0.22*	*0.27*	*49.66*	*2.4*	*1268.1*	*2.8*	*11.3*	*0.28*	*40.27*
		EKO	*8.10*	*0.55*	*0.22*	*0.26*	*47.96*	*3.2*	*1097.4*	*4.7*	*10.2*	*0.27*	*39.29*
		EKO	*8.02*	*0.58*	*0.27*	*0.26*	*48.06*	*3.2*	*1161.9*	*4.2*	*11.3*	*0.31*	*39.82*
		EKO	*8.90*	*0.58*	*0.24*	*0.26*	*47.69*	*3.2*	*1152.9*	*4.4*	*12.1*	*0.33*	*43.18*
		EKO	*8.93*	*0.69*	*0.28*	*0.28*	*47.62*	*3.4*	*1145.3*	*4.9*	*11.9*	*0.33*	*46.15*
	WF	*EKO*	*9.04*	*0.58*	*0.22*	*0.26*	*47.85*	*3.2*	*1144.0*	*4.6*	*12.1*	*0.35*	*43.95*
		EKO	*8.81*	*0.57*	*0.24*	*0.26*	*47.89*	*3.1*	*1113.2*	*4.3*	*10.8*	*0.32*	*42.30*
		EKO	*9.26*	*0.63*	*0.23*	*0.27*	*47.80*	*3.3*	*1147.1*	*5.0*	*11.9*	*0.33*	*45.63*
		EKO	*9.55*	*0.68*	*0.35*	*0.28*	*47.63*	*3.3*	*1203.1*	*4.9*	13.2	*0.37*	*47.47*
		EKO	*8.99*	*0.65*	*0.23*	*0.27*	*48.24*	*3.6*	*1159.7*	*5.1*	*12.6*	*0.33*	*45.11*
		EKO	*8.75*	*0.64*	*0.24*	*0.27*	*48.37*	*3.4*	*1166.7*	*4.6*	*11.7*	*0.34*	*46.11*
Well 4	WF	EKO	3.72	0.25	0.23	0.34	51.72	1.5	1542.5	2.5	12.0	0.30	34.76
		EKO	2.43	0.62	0.25	0.31	50.85	2.9	1490.4	7.3	16.3	0.47	58.25
		EKO	2.72	0.67	0.61	0.33	51.28	3.3	1572.2	6.7	17.2	0.47	63.09
	UF	EKO	2.27	0.24	0.20	0.38	50.96	1.7	1529.6	3.1	11.7	0.29	32.44
		EKO	2.51	0.21	0.19	0.36	50.61	1.6	1391.3	2.5	10.6	0.25	29.58
		EKO	2.77	0.29	0.16	0.36	50.56	0.8	1288.1	2.7	10.3	0.26	29.38
		EKO	1.02	0.12	0.19	0.45	52.57	0.9	1483.8	1.4	7.6	0.20	20.19
		EKO	1.23	0.08	0.15	0.45	50.84	0.8	1205.1	1.3	7.0	0.16	17.08
		EKO	1.24	0.09	0.18	0.48	49.77	0.8	1219.4	1.5	6.7	0.15	17.25
		EKO	1.10	0.08	0.15	0.42	50.28	0.8	1162.2	1.4	6.5	0.17	17.00
		EKO	1.30	0.08	0.14	0.42	46.34	0.9	1101.0	1.2	7.1	0.20	17.76
		EKO	2.71	0.26	0.28	0.56	47.79	0.9	1065.6	4.0	10.3	0.29	36.22
		EKO	2.75	0.22	0.29	0.55	47.94	1.5	1177.2	3.3	9.2	0.25	31.12
Well 5	UF	**EKO**	**17.78**	**0.78**	**0.51**	**0.60**	**41.30**	**4.5**	**835.1**	**9.7**	**11.2**	**0.31**	**41.91**
		EKO	*9.48*	*0.35*	*0.56*	*0.66*	*47.45*	*2.0*	*1042.0*	*5.8*	*11.5*	*0.31*	*40.47*
		EKO	**15.51**	**0.63**	**0.48**	**0.59**	**43.45**	**3.3**	**789.9**	**7.8**	**11.6**	**0.31**	**40.74**
		EKO	**16.48**	**0.67**	**0.52**	**0.65**	**42.11**	**3.9**	**851.7**	**10.2**	**11.6**	**0.31**	**41.00**
		EKO	2.58	0.18	0.21	0.72	51.90	0.8	1298.3	3.3	11.7	0.32	41.27
		EKO	2.29	0.17	0.17	0.65	52.87	0.5	1300.8	2.7	11.7	0.32	41.54
		EKO	2.50	0.17	0.16	0.67	52.54	0.6	1310.9	3.0	11.8	0.32	41.80
		EKO	2.54	0.18	0.16	0.65	52.52	0.5	1321.6	2.7	11.8	0.32	42.07
		TOR	2.13	0.22	0.14	0.50	50.90	0.8	1083.3	3.7	11.9	0.32	42.33
		TOR	2.05	0.20	0.14	0.90	51.59	0.7	1019.5	3.3	11.9	0.32	42.60
		TOR	2.09	0.24	0.20	0.52	52.71	0.7	1149.0	3.0	11.9	0.32	42.87
		TOR	2.16	0.22	0.12	0.50	52.02	0.8	1148.5	4.2	12.0	0.33	43.13

Table 4
Major, minor and trace element concentrations in samples from wells 6–11; HC – hydrocarbon; NON-R – non-reservoir samples; RES – reservoir samples; dl - detection limit; bdl - below detection limit; italics – marly chalk; bold – marl.

Well	HC content	Fm	SiO2	Al2O3	Fe2O3	MgO	CaO	Rb	Sr	Zr	Y	Ho	ΣREE
			%	%	%	%	%	PPM	PPM	PPM	PPM	PPM	PPM
		dl	0.01	0.01	0.01	0.01	0.01	0.1	0.5	0.1	0.1	0.02	
Well 6	NON-R	**EKO**	**11.25**	**0.36**	**0.27**	**0.42**	**47.64**	**1.5**	**1335.5**	**3.7**	**6.5**	**0.17**	**21.75**
		EKO	2.72	0.25	0.2	0.29	52.15	1.2	1449.9	2.9	10.9	0.23	41.73
	RES	EKO	4.14	0.21	0.02	0.40	51.27	1.3	1342.3	7.8	7.9	0.22	22.51
		TOR	1.07	0.10	0.23	0.28	53.98	0.4	1659.9	2.3	9.9	0.29	27.18
		TOR	1.40	0.20	0.09	0.34	54.09	1.1	1576.6	4.4	10.2	0.25	27.54
		TOR	1.60	0.21	0.02	0.33	53.94	0.9	1699.0	5.1	9.0	0.20	24.94
		TOR	1.33	0.30	0.14	0.33	53.96	1.2	2150.2	2.1	9.9	0.25	29.01
		TOR	1.40	0.29	0.02	0.31	54.28	1.4	1847.2	3.9	8.4	0.22	25.00
Well 7	NON-R	**EKO**	**21.49**	**3.59**	**1.45**	**0.72**	**38.41**	**23.5**	**1036.0**	**27.8**	**13.2**	**0.42**	**75.45**
		EKO	**14.35**	**1.74**	**0.75**	**0.39**	**44.41**	**11.4**	**1200.8**	**13.7**	**11.3**	**0.33**	**54.64**
		EKO	**25.13**	**2.48**	**0.99**	**0.48**	**37.97**	**12.8**	**1013.8**	**15.5**	**16.8**	**0.56**	**90.24**
		EKO	**10.92**	**0.53**	**0.26**	**0.17**	**47.35**	**3.2**	**1177.6**	**4.7**	**9.4**	**0.27**	**32.53**
		EKO	**19.45**	**1.69**	**0.62**	**0.37**	**43.48**	**7.5**	**1097.9**	**8.7**	**13.9**	**0.42**	**70.30**
		EKO	**10.32**	**0.29**	**0.27**	**0.21**	**48.48**	**1.8**	**1255.6**	**3.1**	**8.3**	**0.24**	**28.96**
		EKO	**16.96**	**1.22**	**0.51**	**0.30**	**44.73**	**6.4**	**1228.2**	**9.1**	**11.3**	**0.34**	**52.21**
		EKO	*8.88*	*0.94*	*0.33*	*0.20*	*47.83*	*4.8*	*1088.0*	*7.7*	*9.5*	*0.27*	*38.73*
		EKO	*5.23*	*0.59*	*0.25*	*0.16*	*50.47*	*2.7*	*1214.2*	*4.6*	*8.3*	*0.23*	*30.46*
		EKO	*5.95*	*0.54*	*0.23*	*0.17*	*50.01*	*2.6*	*1147.4*	*3.9*	*8.7*	*0.22*	*30.26*
		EKO	**11.90**	**1.16**	**0.38**	**0.26**	**46.78**	**6.2**	**1209.5**	**7.9**	**13.3**	**0.36**	**51.21**
		EKO	**11.40**	**1.45**	**0.44**	**0.30**	**47.97**	**8.0**	**1181.0**	**9.4**	**13.8**	**0.43**	**61.39**
		EKO	**22.21**	**3.09**	**1.01**	**0.71**	**39.02**	**14.0**	**1109.8**	**20.4**	**22.2**	**0.76**	**116.49**
		EKO	**15.74**	**0.72**	**0.47**	**0.27**	**45.12**	**2.7**	**1430.3**	**7.4**	**19.9**	**0.56**	**80.20**
		EKO	**34.95**	**1.94**	**0.74**	**0.46**	**33.13**	**8.5**	**1128.8**	**11.9**	**18.5**	**0.55**	**85.41**
		EKO	**37.23**	**3.70**	**1.41**	**0.77**	**29.22**	**19.2**	**928.1**	**24.5**	**11.0**	**0.41**	**74.68**
		EKO	**13.96**	**0.75**	**0.50**	**0.36**	**46.26**	**4.7**	**1501.1**	**6.8**	**13.8**	**0.45**	**56.99**
		EKO	**11.62**	**1.72**	**0.81**	**0.50**	**45.79**	**9.1**	**1572.9**	**10.3**	**15.0**	**0.43**	**69.61**
		EKO	**22.13**	**3.44**	**1.65**	**0.84**	**38.21**	**17.5**	**1349.5**	**21.8**	**18.6**	**0.62**	**101.89**
	RES	**EKO**	**34.83**	**1.64**	**0.47**	**0.35**	**33.70**	**3.8**	**1343.9**	**7.2**	**9.4**	**0.29**	**49.15**
		EKO	**39.92**	**6.34**	**1.00**	**1.08**	**25.47**	**45.1**	**1207.0**	**61.2**	**28.8**	**0.91**	**170.43**
		EKO	**13.60**	**1.72**	**1.22**	**0.68**	**46.23**	**6.7**	**1130.2**	**7.8**	**15.7**	**0.49**	**60.56**
		EKO	**10.34**	**1.00**	**0.22**	**0.42**	**48.30**	**3.1**	**1185.6**	**4.4**	**8.3**	**0.27**	**33.39**
		EKO	*9.71*	*0.56*	*0.15*	*0.24*	*48.72*	*2.8*	*1147.0*	*5.7*	*11.0*	*0.29*	*39.53*
		TOR	**10.08**	**0.97**	**0.27**	**0.28**	**48.59**	**5.8**	**1183.0**	**7.1**	**14.1**	**0.40**	**56.69**
		TOR	*6.31*	*0.54*	*0.17*	*0.23*	*50.89*	*2.4*	*1193.0*	*5.7*	*10.6*	*0.29*	*41.68*
		TOR	2.80	0.34	0.09	0.21	53.19	0.8	1517.3	1.8	10.3	0.26	31.55
		TOR	4.09	0.30	0.08	0.19	52.18	1.0	1325.6	2.0	10.2	0.26	32.24
		TOR	3.08	0.25	0.07	0.22	53.13	1.2	1523.7	2.5	9.7	0.24	28.22
		TOR	3.33	0.28	0.08	0.20	52.48	1.1	1525.9	2.0	11.6	0.28	32.59
		TOR	3.35	0.30	0.08	0.21	52.68	1.1	1463.0	9.6	11.3	0.30	31.64
		TOR	3.09	0.19	0.11	0.20	52.32	1.0	1377.8	6.0	12.7	0.31	34.48
		TOR	2.82	0.26	0.08	0.20	53.37	1.3	1400.3	2.7	13.1	0.35	38.50
		TOR	0.60	0.05	0.03	0.20	54.38	0.1	1732.6	0.7	8.4	0.21	18.60
		TOR	1.22	0.11	0.07	0.73	54.32	0.6	1407.6	1.4	9.3	0.23	23.61
		TOR	2.00	0.14	0.11	0.23	52.50	1.3	1309.2	2.8	8.1	0.17	30.12
		TOR	1.06	0.16	0.08	0.35	53.96	0.9	1436.4	1.6	8.9	0.19	24.13
		TOR	1.22	0.20	0.08	0.33	53.94	1.2	1401.4	2.5	9.3	0.23	27.32
		TOR	0.87	0.23	0.09	0.22	54.05	1.2	1329.4	2.2	9.5	0.26	28.60
		TOR	0.99	0.21	0.08	0.23	54.40	1.3	1348.2	1.5	8.5	0.21	23.74
		TOR	1.83	0.47	0.14	0.31	54.12	2.5	1283.1	5.5	11.8	0.33	37.00
		TOR	1.59	0.36	0.09	0.26	53.74	2.0	1290.6	2.3	10.0	0.26	30.68
		TOR	2.44	0.30	0.07	0.32	53.11	2.1	924.4	2.6	8.0	0.89	25.81
		TOR	2.43	0.26	0.10	0.39	53.98	2.0	838.4	3.6	6.8	0.16	22.19
		TOR	2.34	0.34	0.10	0.25	53.33	2.5	1116.5	2.3	8.0	0.20	24.93
		TOR	2.56	0.23	0.11	0.26	52.51	1.6	917.5	6.3	7.3	0.20	21.29
		TOR	2.88	0.56	0.14	0.33	53.18	3.6	1082.2	5.0	10.9	0.32	40.61
Well 8	NON-R	TOR	2.28	0.62	0.10	0.33	53.13	1.5	934.9	2.6	9.0	0.24	29.77
		TOR	0.93	0.17	0.06	0.32	54.61	0.8	939.0	13.4	6.6	0.17	19.45
		TOR	0.93	0.17	0.09	0.33	53.74	0.6	1072.4	2.2	6.4	0.20	20.81
		TOR	0.92	0.16	0.07	0.32	54.38	0.8	846.4	2.0	6.2	0.17	17.99
		HOD	*6.04*	*0.58*	*0.19*	*0.38*	*50.79*	*2.2*	*1261.4*	*3.8*	*12.9*	*0.39*	*54.56*
		HOD	4.76	0.43	0.21	0.34	51.46	2.8	1634.0	4.4	11.8	0.33	50.12
		HOD	3.98	0.61	0.23	0.36	51.62	4.2	1125.1	8.7	11.9	0.36	50.42
		HOD	3.54	0.43	0.18	0.38	51.74	2.4	1103.5	4.1	10.9	0.27	43.74
Well 9	NON-R	TOR	2.17	0.37	0.16	0.30	53.35	1.3	651.8	3.2	8.7	0.21	27.72
		TOR	**14.74**	**1.63**	**0.71**	**0.52**	**44.44**	**12.0**	**900.5**	**19.0**	**15.9**	**0.50**	**81.85**
		TOR	*5.49*	*0.67*	*0.25*	*0.27*	*50.48*	*3.2*	*846.5*	*7.2*	*15.3*	*0.48*	*65.87*
		TOR	4.97	0.93	0.36	0.32	51.18	4.5	1101.2	6.5	14.8	0.48	67.58
Well 10	RES	TOR	1.33	0.17	0.15	0.22	51.55	0.8	819.8	4.5	10.6	0.24	23.09
		TOR	2.22	0.44	0.17	0.25	50.65	2.4	742.6	2.6	9.2	0.19	21.90
	NON-R	TOR	1.09	0.20	0.10	0.29	53.97	1.0	893.9	8.1	5.1	0.12	15.65

(*continued on next page*)

Table 4 (*continued*)

Well	HC content	Fm	SiO2	Al2O3	Fe2O3	MgO	CaO	Rb	Sr	Zr	Y	Ho	ΣREE
			%	%	%	%	%	PPM	PPM	PPM	PPM	PPM	PPM
		dl	0.01	0.01	0.01	0.01	0.01	0.1	0.5	0.1	0.1	0.02	
		HOD	*6.22*	*0.80*	*0.27*	*0.41*	*50.55*	*4.1*	*950.4*	*5.0*	*13.4*	*0.46*	*63.90*
		HOD	2.24	0.33	0.14	0.28	53.16	1.9	870.6	6.8	9.1	0.27	33.92
Well 11	NON-R	TOR	1.55	0.20	0.11	0.33	52.85	1.0	770.7	5.0	6.9	0.16	19.52
		TOR	0.90	0.14	0.07	0.31	53.77	0.7	750.8	4.4	5.2	0.15	15.65
		TOR	0.99	0.14	0.13	0.32	53.18	0.8	865.8	1.5	5.2	0.18	16.94

Table 5
Major, minor and trace element concentrations in samples of insoluble residue from well 3; dl - detection limit; bdl - below detection limit; WF - waterflooded; UF - unflooded.

	Flooding status	Fm	SiO2	Al2O3	Fe2O3	MgO	CaO	Rb	Sr	Zr	Y	Ho	ΣREE
			%	%	%	%	%	PPM	PPM	PPM	PPM	PPM	PPM
		dl	0.01	0.01	0.01	0.01	0.01	0.1	0.5	0.1	0.1	0.02	
IR-Well 3	UF	EKO	74.96	8.73	1.58	1.16	1.18	39.00	96.6	37.80	24.30	0.80	139.82
		EKO	66.87	4.36	0.67	0.61	4.34	20.40	187.2	24.20	26.40	0.78	115.76
		EKO	66.78	5.91	1.02	0.82	3.53	25.20	166.2	32.90	30.50	0.91	145.58
	WF	EKO	72.04	4.88	0.70	0.65	1.43	24.10	119.4	31.20	29.50	0.94	135.37
		EKO	72.07	5.40	0.75	0.69	1.36	25.80	113.5	33.80	29.50	0.91	140.89

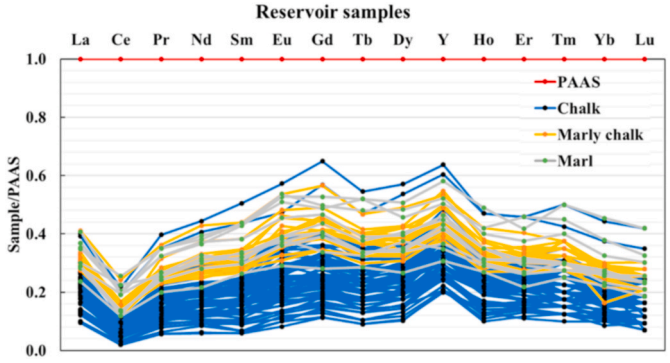

Fig. 5. Shale normalized Yttrium and Rare Earth Element chemistry in selected reservoir chalk, whole rock samples categorized by amount of silica content: chalk (<5% silica, blue lines), marly chalk (5–10% silica, yellow lines) and marls (<10% silica grey lines). (For interpretation of the references to color in this figure legend, the reader is referred to the Web version of this article.)

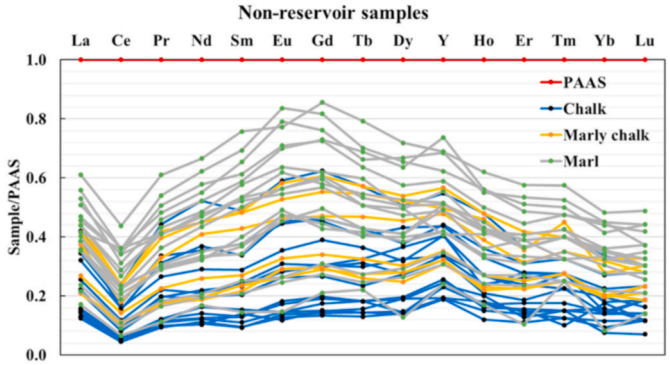

Fig. 6. Shale normalized Yttrium and Rare Earth Element chemistry in selected non-reservoir chalk, whole rock samples categorized by amount of silica content: chalk (<5% silica, blue lines), marly chalk (5–10% silica, yellow lines) and marls (<10% silica grey lines). (For interpretation of the references to color in this figure legend, the reader is referred to the Web version of this article.)

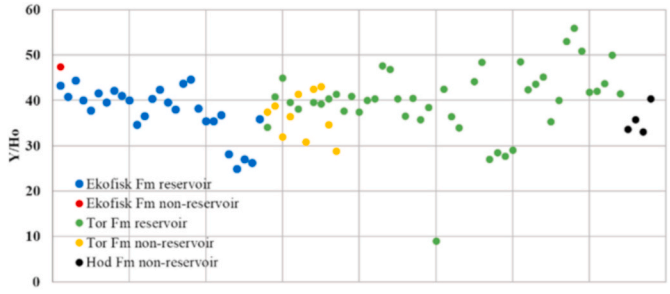

Fig. 7. Y/Ho ratios in clean chalk (<5% silica content) whole-rock samples from all formations: the average for reservoir samples is 38 (Ekofisk Fm) and 40 (Tor Fm). Y/Ho ratios in non-reservoir samples are in average 38 (Tor Fm) and 34 (Hod Fm).

values are definitely below those from on-shore chalk at Stevns Klint (Denmark), but comparable to those from Liège quarry, Belgium (Andersen et al., 2018), Aalborg quarry (Denmark) and Mons basin (Belgium) (average 40, Minde et al., 2018). Several reservoir samples (Tor Formation) show higher values (over 50), which may point to either less clastic input or a less penetrative restricted fluid flow that would have lowered the Y/Ho, or both. This will be studied in the nearest future intensively.

Abundances of sulfur (S) and barium (Ba) are interesting to notice, as well as strontium (Sr). The latter does not always correlate with increased CaO concentrations, which may point to a diagenetic overprint.

All other trace elements are depleted in the chalk samples, while several marly chalk samples show slight enrichments in Pb or Ni. Marls, like shales, or the insoluble residue samples from well 3, contain typical abundances of clastic sediments comparable to the typical Upper Continental crust (after McLennan et al., 2006).

4.6. *Stable isotope geochemistry*

Determined $\delta^{13}C$ values are comparable in all northern, non-reservoir samples, averaging at +1.7‰. Generally, the reservoir probes are slightly enriched in the heavy C isotope (i.e., higher $\delta^{13}C$), compared to the samples from the northern wells, averaging at +2.0‰, but remain within the expected range for unaltered Late Cretaceous

chalk, between 1.0 and 2.5 ‰$_{PDB}$ (Gradstein et al., 2012; Cramer et al., 2009).

Oxygen isotopic composition varies more than the carbon values in all wells, but it follows mainly a negative trend relative to burial depth (Fig. 8, red markers). Reservoir samples register slightly higher $\delta^{18}O$ ratios than the northern well samples, −4.6‰ and −5.0‰ respectively, but are significantly lower than the estimated oxygen isotopic composition for Late Cretaceous chalk ranging between 0 and -1.5‰ (Scholle, 1977; Cramer et al., 2009).

Reservoir samples from the Ekofisk Formation (Fig. 9; blue markers) stand out with higher oxygen isotope ratios (average of −4‰) compared to the rest of the samples (Fig. 9). The $\delta^{13}C$ versus $\delta^{18}O$ cross plot shows sporadic positive covariations, typical for carbonate precipitation in marine/meteoric mixing zone (Allan and Matthews, 1982). Data points from Tor and Hod Formations, from both reservoir and non-reservoir wells scatter considerably and generally show stronger $\delta^{18}O$ disturbance than the Ekofisk reservoir samples.

5. Discussion

5.1. Petrology, mineralogy, and geochemistry

The optical petrography and SEM imaging revealed a sediment composition typical for Upper Cretaceous chalks, consisting of micritic carbonate matrix, microfossils and diverse but subordinated authigenic and detrital minerals. The deposition of coccolithosphores, the space between the whole and disintegrated calcite platelets, are the primary source of porosity that produces a good reservoir rock. The preserved calcite skeletons of foraminifers are efficient in enhancing the chalk porosity, as well as the void left after the dissolution of sponge spicules

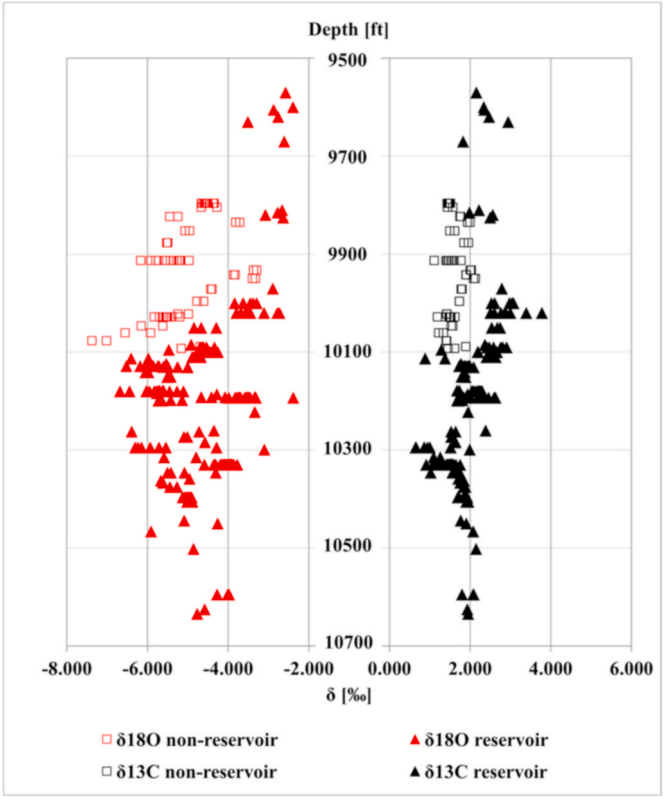

Fig. 8. Oxygen (red markers) and carbon (black markers) stable isotope curves of reservoir (full triangles) and non-reservoir (empty squares) rock samples from shallower (top) to deeper layers (bottom). (For interpretation of the references to color in this figure legend, the reader is referred to the Web version of this article.)

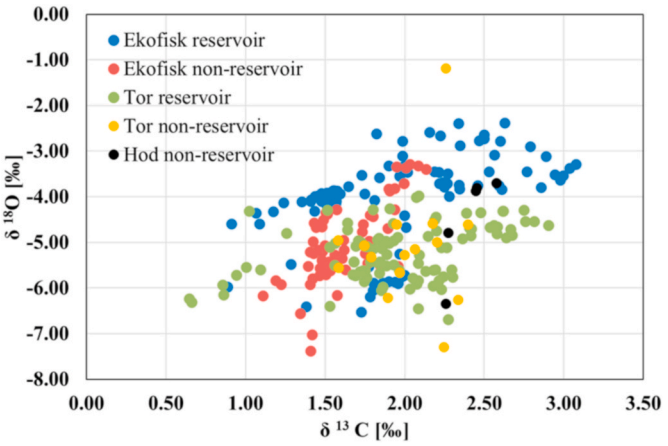

Fig. 9. Cross-plot showing correlation between carbon and oxygen isotope ratios from reservoir and non-reservoir samples. Both reservoir (blue markers) and non-reservoir (red markers) from Ekofisk Formation show a brief positive linear correlation, while the rest of the data points scatter significantly. (For interpretation of the references to color in this figure legend, the reader is referred to the Web version of this article.)

(Figs. 2–4).

Another factor contributing to enhanced porosity and good permeability is the fracturing of the chalk as veins and interconnected crack networks. Field reports show that the vast fracture system at Ekofisk field is responsible for effectively enhancing the reservoir permeability from 1 to 5 mD (matrix permeability) by up to two orders of magnitude (Haper and Shaw, 1974; Brown, 1987; Sulak and Danielsen, 1989; Teufel and Rhett, 1992). Yet, calcite cementation and partial secondary mineralization of fractures such as observed in this study (Fig. 4) can obstruct fluid flow, hence reducing permeability (Agrawal et al., 1997). This is important aspect to consider in further studies and modeling of porosity and permeability of fractured chalk at reservoir scale exposed to mechanical and thermochemical influence.

On the other hand, diagenetic processes reduce porosity, as often fractures, dissolved sponge spicules, and microfossils are entirely or partially filled by *in situ* precipitated calcite, or spar calcite cement. The stratigraphic lower reservoir chalk from Ekofisk Formation shows microfossils that are often deformed, or have collapsed walls, and filled with matrix material. This may be an effect of burial, or deformation related to tectonic activity, but based on the scarce geological information available, this cannot be evaluated. Nevertheless, compaction would normally reduce porosity in such a fragile rock. Hence, a process counteracting this geological process had to be present in early diagenetic phases (Scholle, 1977).

The geochemistry of the chalk samples (Tables 3 and 4) showed, among the major elements, only minute enrichment in MgO in some samples and a typical limestone composition with low silica content. Quartz is the main non-carbonate phase with only few other silicates. Marly chalks and moreover marls are enriched in clastic material. However, no significant enrichments in any lithotype could be observed, which would point to a specific geological process, in terms of a changing depositional environment; the samples seem to be rather comparable. The existence of a higher clastic input may be related to tectonic movements and a short interruption of carbonate production. The latter can be caused by colder times and the former by exhumation of older clastic-dominated rock formations. However, no provenance studies have been made on the clastic material within chalk.

Nonetheless, chalks in the reservoir wells differ strongly in regards to the clastic contamination, with some wells only represented by marly chalks and marls within the Ekofisk Formation. The introduction of clastic material seems to start mostly at the bottom of the Ekofisk Formation and rarely already during deposition of the Tor Formation

(Tables 3 and 4). This variation is of utmost importance when modelling or estimating rock-fluid interactions in possible reservoirs.

Rare earth elements (REE) are sensitive monitors for a variation of geological aspects. The overall sum of REE for clean carbonates should be very low (close to the lower limit of detection) and higher values, like in this case, are an indication of terrestrial input and/or secondary fluid flow (Frimmel, 2009). The even lower sum of REE found in mantle rocks (Ullah et al. 2020a, 2020b) points to an origin of the REE from non-mantle sources. Crustal abundance of REE however, may explain the abundance in the chalk deposits studied here. Contamination with detrital materials, especially terrigenous clay minerals, can effectively alter REE signature patterns for marine deposits, increase the total REE (ΣREE) as well as the concentration of Zr, Th and Al (Frimmel, 2009).

Clastic input can undoubtedly be seen in the SEM, XRD and the whole-rock geochemistry. Besides kaolinite, the XRD, SEM-BSE-EDS analyses showed a large variety of clay minerals and detrital grains. However, Al_2O_3 concentrations are low as such that future studies need to determine accurately the amount and type of clastic material in the different reservoirs or wells. Clays can possibly be introduced either by alteration of feldspar or as alteration product of volcanic glass, epiclastic material from explosive volcanism. As the main volcanic sources during the opening of the Atlantic Ocean were of mafic composition, subaerial explosive volcanism may have been rare to absent, and therefore the clays related to the alteration of glass are rather linked to sub-marine explosive processes and relicts of hyaloclastites.

Nevertheless, most of the chalk samples show typical geochemical patterns for limestones precipitates from seawater (Figs. 5 and 6). Y/Ho ratios, however, vary and mainly show a significant influence of non-seawater within the chalks (Bau, 1996). The origin of this fluid-flow and the timing of its circulation is unknown. The sparse appearance of secondary growth of minerals and low cementation points to an incomplete and only slight overprint.

The stable isotopic analyses of C and O show results typical for a marine depositional environment. Carbon isotope ratios align well with primary trends for Upper Cretaceous stages (Fig. 10). Slightly lower values may be caused either by mixing of carbonate phases from different depositional environments, when the chalk is brecciated thus reworked, or by enrichment of organic carbon (i.e., higher ^{12}C) from meteoric origin, or they might reflect a colder environment, related to the water depth in which the carbonate precipitated. However, the narrow $\delta^{13}C$ variability compared to the $\delta^{18}O$ outrules strictly meteoric diagenesis and local positive C–O covariation suggests rather a marine-meteoric mixing zone (Allan and Matthews, 1982). The low Y/Ho ratios also point to the influence of meteoric/hydrothermal water and support this interpretation.

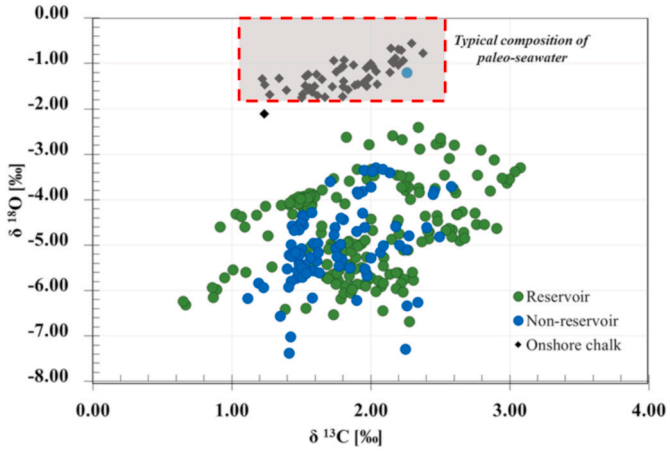

Fig. 10. Cross plot of carbon and oxygen isotopic composition of offshore and onshore chalk from Danish outcrop locations (Andersen et al., 2018); the dashed red frame marks the expected plot area for undisturbed Cretaceous carbon and oxygen stable isotopes (after Gradstein et al., 2012). (For interpretation of the references to color in this figure legend, the reader is referred to the Web version of this article.)

Oxygen isotopes on the other hand, are not primary, and considerable deviation from the Upper Cretaceous trends (i.e, 0 to −1.5‰) is seen in all samples. Previous studies showed that oxygen isotopes are subject to burial diagenesis, becoming increasingly negative with depth (Hudson, 1977; Scholle, 1977; Allan and Matthews, 1982), a trend seen here as well (Fig. 8), although the alteration is not as severe, considering the burial depth.

Additionally, the marine-meteoric mixing zone, which may have influenced the carbon isotopes, and is also reflected in rather low Y/Ho ratios (Fig. 7), can also explain the oxygen isotopes pattern, as strongly negative $\delta^{18}O$ values imply a different water input than of marine origin. Moreover, water temperature can influence oxygen isotopes, and warmer average temperatures can lower $\delta^{18}O$ values. Thus, paleo-temperature fluctuations, or meteoric water input with different thermal gradient can plausibly explain the disturbed oxygen isotopes.

Analyses of the chemical composition of the ancient seawater show that the distribution of the REE does not suffer substantial changes compared to the present-day seawater pattern (Shields and Webb, 2004). Were there no other fluids besides the original seawater environment, the chalk should have retained the main characteristics of the original fluid environment. Although in this case the REE and Y pattern follows the typical open marine seawater signature, the overall depletion is less than what is expected for (pure) chalk deposits. The hydrothermal influence is clear in all wells, underlined by the presence of numerous minerals typically related to such an environment (pyrite, albite, sphalerite, etc.).

Further arguments supporting the presence of a secondary fluid are based on the Y and Ho concentrations, as they should have a positive linear correlation when chemical processes and not detrital ones dominate their abundance. The positive linear correlation between the abundance of the two elements in the geochemistry results indicates that the fractionation took place in a marine environment. However, the low Y/Ho ratios (average 40, Fig. 7) seen in the North Sea reservoir chalk are much below what is typical for seawater (Nozaki et al., 1997; Bau and Dulski, 1996, 1999), and therefore reflect the presence of another fluid, assumingly fresh, meteoric/hydrothermal water, or intraformational water stored in rock successions. Such a fluid flow may have been triggered by the emergence of magma to produce the large volumes of extrusions during the Early Paleogene. This is, however, only speculation and needs to be substantiated with study of trapped seawater in lava vesicles of the Cenozoic extrusive rocks.

5.2. Diagenetic overprint

The occurrence of dolomite points to either a significant fluid flow to initiate dolomitization or to a slowly developing diagenesis. New dolomite crystals were detected in all thin sections from the Ekofisk area, mostly in pores and along fractures, but not in the northern, non-reservoir wells (Fig. 4).

Clay minerals are most readily adjusted to the changes in the chemical conditions during burial. XRD analyses can identify such diagenetic changes, by considering the change in the mineral assemblage (e.g., from smectite to illite downwards). The presence of illite was observed in the XRD patterns (and confirmed with SEM analysis in Fig. 3), but only in a few samples as a minor contributor to the non-carbonate mineral assemblage.

Areas in which pores are partly filled with secondary, re-worked material are observed (Fig. 4), but this does not seem to be a significant, regional event rather active on a local area as geochemical data addressed.

Using stable isotope values as monitors for the influence of diagenetic processes when the ratios are not anymore primary has been proposed in various contributions (compiled in Gomez Peral et al.,

2007), most commonly corroborated with values from Mn, Fe, Mn/Sr ratio, 1000*Sr/Ca, Fe/Sr and Rb/Sr. According to this evaluation, none of the chalk samples in this study are pointing to any significant diagenetic overprint. Marly chalks and marls are affected by clastic input and the values of those samples cannot be considered. The only exception are Sr/Ca ratios which are definitely too high and can be affected by Sr-isotopes. The enrichment of Sr over Ca, which should rather have a character of positive correlation points to another Sr-bearing source, like baryte. This may be part of the rock either primary or introduced during migration of hydrocarbons and/or added during the drilling process. However, as all other indicators do not point to a strong diagenesis, we state that the change of the stable oxygen isotopes is not dominated by diagenetic processes. The amount of clastic detritus, not abundant enough to cause all the alterations seen in the geochemistry of the chalk, supports the assumption of another contaminant, most likely a secondary fluid, which also may comprise sufficient Mg to trigger dolomitization. Still, magmatic activity may have played a substantial role. Therefore, we interpret the diagenetic overprint as visible but rather very low and it varies depending on the local geological setting which allowed a deeper burial in some areas because of syn-depositional tectonic movements producing slightly more accommodation space for overburden.

5.3. Influence of hydrocarbons and EOR fluids

It is unlikely that the presence of hydrocarbon fluids was the cause of the negative $\delta^{18}O$, as both the reservoir (Fig. 10, green markers) and the non-reservoir successions (blue markers) show similar oxygen isotope pattern. By comparison, a number of Late Cretaceous samples of onshore chalk from Aalborg, Stevns Klint, Liège and Mons Basin (Andersen et al., 2018) show isotopic values in concordance with the typical paleo-seawater isotopic composition (Fig. 10; black diamonds).

A negative trend with depth is observed in both reservoir and non-reservoir samples (Fig. 8) which may reflect burial lithification (Hudson, 1977). However, generally higher oxygen isotope ratios in reservoir compared to non-reservoir samples might be related to the presence of hydrocarbons. It may be that the processes that stabilized the chalk (early hydrocarbon entry, overpressuring, Nygaard et al., 1983; Brasher and Vagle, 1996) and were responsible for the early change of the REE concentrations, also retarded further change in the O isotope ratios during early, very low grade diagenesis.

The similarity between REE values of unflooded and flooded high porosity chalk (Table 3) excludes that artificial flooding events are decisive for the observed negative oxygen ratio shift, which is therefore interpreted as natural, rather than anthropologic.

Field observations and laboratory studies confirm that NCS chalk is prone to mineralogical and textural changes when in contact with reactive EOR brines, and the effects of rock-fluid interactions are enhanced with higher injecting brine temperature (Austad et al., 2008; Madland et al., 2011; Megawati et al., 2015). The main mineralogical alterations are explained in terms of calcite dissolution and precipitation of new minerals such as magnesite, or anhydrite (Madland et al., 2011; Minde et al., 2018) and mineral alteration is most obvious close to the injection inlet (Minde et al., 2018; Kallesten et al., 2020). Production-related mineral alteration is possibly observed here as well. XRD analyses distinguished between flooded and unflooded samples in well 1, where the waterflooded cores had less calcite than the unflooded cores. Flooding temperature did not seem to make a difference, as both hot and cold waterflooded samples contained a similar amount of calcite.

However, samples from other wells that have been exposed to seawater injection do not show the same correlation. Most of the samples from well 2 as an example, although flooded, contained almost exclusively calcite. SEM analyses show that the mineral assemblage is similar in all reservoir wells and that the mineral and textural differences (e.g., presence of dolomite, pore morphology) are rather depositional, independent of flooding status (Figs. 3 and 4). Geochemistry results confirm this observation.

This does not necessarily rule out the effect of EOR fluids on chalk mineralogy, and the newly precipitated minerals might be more clearly seen closer to the brine injectors. However, this can only be resolved with a large sample set including well cores and drilled chalk less affected by artificial fluids.

The low diagenetic overprint, the presence of dolomite together with the often-high amount of clastic material within the chalk is of importance when testing onshore chalk as equivalent for the reservoir rocks in the context of smart water injection for EOR processes. Studies show that dolomite is less reactive to EOR fluids such as seawater than calcite (Shariatpanahi et al., 2016). Further, pure chalk has a slower reaction rate to seawater than chalk with higher non-carbonate content, particularly clays (Madland et al., 2011). The introduction of clastic material into the Ekofisk Formation, often the host of hydrocarbon reservoirs, seems to be diachron and variable in its intensity (Tables 3 and 4). This variation is a very difficult issue when EOR techniques are applied and should be considered carefully.

7. Conclusions

Mineralogically, reservoir chalks from Ekofisk consist mainly of calcite; the silica is stored mostly in quartz and its abundance varies considerably (1–10%). Corroborated results from XRD, BSE-SEM-EDS and geochemistry indicate the presence of other non-carbonate mineral phases like illite, smectite, kaolinite, which confirms a significant clastic input. This is a possible cause for the higher REE concentrations and lower Y/Ho ratios (30–40) than expected in marine seawater precipitates, and it may be triggered by the syn-depositional introduction of hydrothermal fluids or meteoric water.

Diagenesis that took place may have caused growth of dolomite and weak cementation; the estimation of the diagenetic grade is not accurately established, but it is estimated to be very low. Diagenetic dolomite occurs together with sparse cementation. The absence of significant changes in elemental ratios and other chemical elements used for monitoring diagenetic processes, in addition to the similarity of geochemical and isotope geochemical values in all chalk samples, point to a low diagenetic overprint and is associated with the effect of a circulation fluid which affected the rocks and their geochemical and isotopic composition. This fluid may be of meteoric origin mixed with existing formation water; it may also have had sufficient Mg concentration to facilitate dolomite growth, and stabilized the rock, assisting in producing the reservoir at Ekofisk.

The non-reservoir chalk samples show similar characteristics as the reservoir samples in terms of sediment composition, textures, and mineralogy. Both lithotypes, with and without hydrocarbon accumulations, are clearly affected by a post-depositional process, which changed the oxygen isotope ratios to more negative values compared to many onshore chalk exposures, therefore ruling out hydrocarbons as possible cause.

There is no clear indication of chemical and mineral alteration due to EOR flooding of the reservoir chalk, possibly because the studied samples were far enough from the injectors where such effects would be more evident. Further studies on larger sample sets including flooded and unflooded fractured reservoir chalk can determine the spatial and temporal distribution of EOR fluid effects when the water chemistry, distance to the injectors, injection rate and time are known. Such data, together with knowledge of the North Sea reservoir chalk characteristics (typical Upper Cretaceous marine deposits, low diagenetic overprint, presence of dolomite and variable clastic input) are instrumental when considering data transfer and applicability of results from outcrop chalk research to the North Sea reservoir chalk context. It also offers a unique insight potential EOR methods and can contribute to increased accuracy of chalk reservoir models.

Author credit statement

E.I. Kallesten: conceptualization, management, investigation, formal analyses, interpretation, data visualization, writing. U. Zimmermann: supervision, sample provision, conceptualization, geochemical interpretation, writing. M. V. Madland: supervision, sample provision, conceptualization, validation, review and editing. Silvana Bertolino: analyses and synthesis of data, writing and editing. Edvard Omdal: supervision, resources provision, conceptualization, review and editing. P. Ø. Andersen: supervision, critical review, revision commentaries, visualization.

Declaration of competing interest

The authors declare that they have no known competing financial interests or personal relationships that could have appeared to influence the work reported in this paper.

Acknowledgements

The authors acknowledge the Research Council of Norway and the industry partners, ConocoPhillips Skandinavia AS, Aker BP ASA, Vår Energi AS, Equinor ASA, Neptune Energy Norge AS, Lundin Norway AS, Halliburton AS, Schlumberger Norge AS, and Wintershall DEA, of The National IOR Centre of Norway for support.

References

Agarwal, B., Allen, L.R., Farrell, H.E., 1997. Ekofisk Field reservoir characterization: mapping permeability through facies and fracture intensity. SPE Form. Eval. 12 (4), 227–234. https://doi.org/10.2118/35527-PA.

Allan, J.R., Matthews, R.K., 1982. Isotope signatures associated with early meteoric diagenesis. Sedimentology 29 (6), 797–817. https://doi.org/10.1111/j.1365-3091.1982.tb00085.x.

Andersen, P.Ø., Wang, W., Madland, M.V., Zimmermann, U., Korsnes, R.I., Bertolino, S. R.A., Gilbricht, S., 2018. Comparative study of five outcrop chalks flooded at reservoir conditions: chemo-mechanical behaviour and profiles of compositional alteration. Transport Porous Media 121 (1), 135–181. https://doi.org/10.1007/s11242-017-0953-6.

Austad, T., Strand, S., Madland, M.V., Puntervold, T., Korsnes, R.I., 2008. Seawater in chalk: an EOR and compaction fluid. SPE Reservoir Eval. Eng. 11 (4), 648–654. https://doi.org/10.2118/118431-PA.

Bau, M., 1996. Controls on the fractionation of isovalent trace elements in magmatic and aqueous systems: evidence from Y/Ho, Zr/Hf, and lanthanide tetrad effect. Contrib. Mineral. Petrol. 123 (3), 323–333. https://doi.org/10.1007/s004100050159.

Bau, M., Dulski, P., 1996. Distribution of yttrium and rare-earth elements in the penge and kuruman iron-formations, transvaal supergroup, South Africa. Precambrian Res. 79 (1–2), 37–55. https://doi.org/10.1016/0301-9268(95)00087-9.

Bau, M., Dulski, P., 1999. Comparing yttrium and rare earths in hydrothermal fluids from the Mid-Atlantic Ridge: implications for Y and REE behaviour during near-vent mixing and for the Y/Ho ratio of Proterozoic seawater. Chem. Geol. 155 (1–2), 77–90.

Bau, M., Alexander, B., 2006. Preservation of primary REE patterns without Ce anomaly during dolomitization of Mid-Paleoproterozoic limestone and the potential re-establishment of marine anoxia immediately after the "Great Oxidation Event". S. Afr. J. Geol. 109 (1–2), 81–86. https://doi.org/10.1016/S0009-2541(98)00142-9.

Bjørlykke, K., Høeg, K., 1997. Effects of burial diagenesis on stresses, compaction and fluid flow in sedimentary basins. Mar. Petrol. Geol. 14 (3), 267–276. https://doi.org/10.1016/S0264-8172(96)00051-7.

Brasher, J.E., Vagle, K.R., 1996. Influence of lithofacies and diagenesis on Norwegian North Sea chalk reservoirs. AAPG Bull. 80 (5), 746–768. https://doi.org/10.1306/64ED88AE-1724-11D7-8645000102C1865D.

Brown, D.A., 1987. The flow of water and displacement of hydrocarbons in fractured chalk reservoirs. Geological Society, London, Special Publications 34 (1), 201–218. https://doi.org/10.1144/GSL.SP.1987.034.01.14.

Cramer, B.S., Toggweiler, J.R., Wright, J.D., Katz, M.E., Miller, K.G., 2009. Ocean overturning since the Late Cretaceous: inferences from a new benthic foraminiferal isotope compilation. Paleoceanography 24 (4). https://doi.org/10.1029/2008PA001683.

D'Heur, M., 1991. West Ekofisk field, Norway, central graben, North Sea (1). AAPG (Am. Assoc. Pet. Geol.) Bull. 75 (5), 946–968. https://doi.org/10.1306/0C9B28A3-1710-11D7-8645000102C1865D.

Dunham, R.J., 1962. Classification of carbonate rocks according to depositional textures. In: Classification of Carbonate Rocks. AAPG Mem, pp. 108–121.

Egeberg, P.K., Saigal, G.C., 1991. North Sea chalk diagenesis: cementation of chalks and healing of fractures. Chem. Geol. 92 (4), 339–354. https://doi.org/10.1016/0009-2541(91)90078-6.

Faleide, J.I., Bjørlykke, K., Gabrielsen, R.H., 2010. Geology of the Norwegian continental shelf. In: Bjørlykke, K. (Ed.), Petroleum Geoscience: from Sedimentary Environments to Rock Physics. Springer-Verlag, Berlin Heidelberg, pp. 470–480.

Frimmel, H.E., 2009. Trace element distribution in Neoproterozoic carbonates as palaeoenvironmental indicator. Chem. Geol. 258 (3–4), 338–353. https://doi.org/10.1016/j.chemgeo.2008.10.033.

Gennaro, M., Wonham, J.P., Sælen, G., Walgenwitz, F., Caline, B., Faÿ-Gomord, O., 2013. Characterization of dense zones within the danian chalks of the Ekofisk field, Norwegian North Sea. Petrol. Geosci. 19 (1), 39–64. https://doi.org/10.1144/petgeo2012-013.

Gradstein, F.M., Ogg, J.G., Schmitz, M., Ogg, G., 2012. The Geologic Time Scale. Elsevier, Oxford, UK, pp. 181–232.

Harper, M.L., Shaw, B.B., 1974. Cretaceous-tertiary carbonate reservoirs in the north Sea: offshore North Sea technology conference. Stavanger, Norway, Paper G IV/ 4, 20.

Herrington, P.M., Pederstad, K., Dickson, J.A.D., 1991. Sedimentology and diagenesis of resedimented and rhythmically bedded chalks from the eldfisk field, North Sea central graben (1). AAPG (Am. Assoc. Pet. Geol.) Bull. 75 (11), 1661–1674. https://doi.org/10.1306/0C9B29CF-1710-11D7-8645000102C1865D.

Hjuler, M.L., Fabricius, I.L., 2009. Engineering properties of chalk related to diagenetic variations of Upper Cretaceous onshore and offshore chalk in the North Sea area. J. Petrol. Sci. Eng. 68 (3–4), 151–170. https://doi.org/10.1016/j.petrol.2009.06.005.

Howie, R.A., Zussman, J., Deer, W., 1992. An Introduction to Rock-Forming Minerals. Longman.

Hudson, J.D., 1977. Stable isotopes and limestone lithification. J. Geol. Soc. 133 (6), 637–660. https://doi.org/10.1144/gsjgs.133.6.0637.

Jensen, T.B., Harpole, K.J., Østhus, A., 2000. EOR screening for Ekofisk. In: SPE European Petroleum Conference. Society of Petroleum Engineers. https://doi.org/10.2118/65124-MS.

Kallesten, E., Andersen, P.Ø., Berawala, D.S., Korsnes, R.I., Madland, M.V., Omdal, E., Zimmermann, U., 2020. Modeling of permeability and strain evolution in chemical creep compaction experiments with fractured and unfractured chalk cores conducted at reservoir conditions. SPE J. 25 (5), 2710–2728. https://doi.org/10.2118/197371-PA.

Madland, M.V., Hiorth, A., Omdal, E., Megawati, M., Hildebrand-Habel, T., Korsnes, R.I., et al., 2011. Chemical alterations induced by rock–fluid interactions when injecting brines in high porosity chalks. Transport Porous Media 87 (3), 679–702. https://doi.org/10.1007/s11242-010-9708-3.

McLennan, S.M., Taylor, S.R., Henning, S.R., 2006. Composition, differentiation, and evolution of continental crust: constraints from sedimentary rocks and heat flow. In: Brown, M., Rushmer, T. (Eds.), Evolution and Differentiation of the Continental Crust. Cambridge University Press, New York, pp. 92–134.

Megawati, M., Madland, M.V., Hiorth, A., 2015. Mechanical and physical behavior of high-porosity chalks exposed to chemical perturbation. J. Petrol. Sci. Eng. 133, 313–327. https://doi.org/10.1016/j.petrol.2015.06.026.

Minde, M.W., Zimmermann, U., Madland, M.V., Korsnes, R.I., Schulz, B., Audinot, J.N., 2016. Fluid–flow during EOR experiments in chalk: insights using SEM–MLA, EMPA and Nanosims Applications. In: International Symposium of the Society of Core Analysts. Colorado, USA, pp. 21–26.

Minde, M.W., Wang, W., Madland, M.V., Zimmermann, U., Korsnes, R.I., Bertolino, S.R., Andersen, P.Ø., 2018. Temperature effects on rock engineering properties and rock-fluid chemistry in opal-CT-bearing chalk. J. Petrol. Sci. Eng. 169, 454–470. https://doi.org/10.1016/j.petrol.2018.05.072.

Nozaki, Y., Zhang, J., Amakawa, H., 1997. The fractionation between Y and Ho in the marine environment. Earth Planet Sci. Lett. 148 (1–2), 329–340. https://doi.org/10.1016/S0012-821X(97)00034-4.

Nygaard, E., Lieberkind, K., Frykman, P., 1983. Sedimentology and reservoir parameters of the chalk group in the Danish central graben. In: Petroleum Geology of the Southeastern North Sea and the Adjacent Onshore Areas, pp. 177–190. https://doi.org/10.1007/978-94-009-5532-5_17.

Peral, L.E.G., Poiré, D.G., Strauss, H., Zimmermann, U., 2007. Chemostratigraphy and diagenetic constraints on neoproterozoic carbonate successions from the sierras bayas group, tandilia system, Argentina. Chem. Geol. 237 (1–2), 109–128. https://doi.org/10.1016/j.chemgeo.2006.06.022.

Scholle, P.A., 1977. Chalk diagenesis and its relation to petroleum exploration: oil from chalks, a modern miracle? AAPG (Am. Assoc. Pet. Geol.) Bull. 61 (7), 982–1009. https://doi.org/10.1306/C1EA43B5-16C9-11D7-8645000102C1865D.

Shariatpanahi, S.F., Hopkins, P., Aksulu, H., Strand, S., Puntervold, T., Austad, T., 2016. Water based EOR by wettability alteration in dolomite. Energy & Fuels 30 (1), 180–187. https://doi.org/10.1021/acs.energyfuels.5b02239.

Shields, G.A., Webb, G.E., 2004. Has the REE composition of seawater changed over geological time? Chem. Geol. 204 (1–2), 103–107. https://doi.org/10.1016/j.chemgeo.2003.09.010.

Stoddart, D.P., Hall, P.B., Larter, S.R., Brasher, J., Li, M., Bjorøy, M., 1995. The reservoir geochemistry of the Eldfisk field, Norwegian North Sea. Geological Society, London, Special Publications 86 (1), 257–279. https://doi.org/10.1144/GSL.SP.1995.086.01.15.

Strand, S., Hjuler, M.L., Torsvik, R., Pedersen, J.I., Madland, M.V., Austad, T., 2007. Wettability of chalk: impact of silica, clay content and mechanical properties. Petrol. Geosci. 13 (1), 69–80. https://doi.org/10.1144/1354-079305-696.

Sulak, R., Danielsen, J., 1989. Reservoir aspects of Ekofisk subsidence. J. Petrol. Technol. 41 (7), 709–716. https://doi.org/10.4043/5618-MS.

Sylte, J.E., Thomas, L.K., Rhett, D.W., Bruning, D.D., Nagel, N.B., 1999. January. Water induced compaction in the Ekofisk field. In: SPE Annual Technical Conference and Exhibition. Society of Petroleum Engineers. https://doi.org/10.2118/56426-MS.

Talukdar, M.S., Torsaeter, O., 2002. Reconstruction of chalk pore networks from 2D backscatter electron micrographs using a simulated annealing technique. J. Petrol. Sci. Eng. 33 (4), 265–282. https://doi.org/10.1016/S0920-4105(02)00148-1.

Taylor, S.R., McLennan, S.M., 1981. The composition and evolution of the continental crust: rare earth element evidence from sedimentary rocks. Phil. Trans. Roy. Soc. Lond. Math. Phys. Sci. 301 (1461), 381–399. https://doi.org/10.1098/rsta.1981.0119.

Teufel, L.W., Rhett, D.W., 1992. Effect of reservoir stress path on permeability of fractures in chalk. In: Proc. 4th North Sea Chalk Symposium..

UIIah, Z., Shah, M.T., Siddiqui, R.H., Lian, D.Y., Khan, A., 2020a. Petrochemistry of high-Cr and high-Al chromitites occurrences of dargai complex along indus suture zone, northern Pakistan. Episodes Jouranl of International Geoscience 43 (2), 689–709 https://doi.org/10.l88l4/epiiugs/2020/020045.

UIIah, Z., Li, J.W., Robinson, P.T., Wu, W., Khan, A., Dac, N.X., Adam, M.M.A., 2020b. Mineralogy and geochemistry of peridotites and chromitites in the jijal complex ophiolite along the main mantle thrust (MMT or indus suture zone) north Pakistan. Lithos 366, 105566. https://doi.org/10.1016/j.lithos.2020.l05566.

Van Den Bark, E., Thomas, O.D., 1981. Ekofisk: first of the giant oil fields in Western Europe. AAPG (Am. Assoc. Pet. Geol.) Bull. 65 (11), 2341–2363. https://doi.org/10.1306/03B59995-16D1-11D7-8645000102C1865D.